10
Special Topics

This chapter deals with several techniques to solve some problems of particular interest in multibody simulation that have not been considered in other chapters. These techniques are neither very sophisticated nor trivial. However, they may be very useful at the time of solving practical or real problems.

The first problem to be considered in this chapter is a way to model *Coulomb friction* in a dynamic simulation. This approach to friction forces and energy dissipation is more accurate in many practical cases than the viscous friction model, but it is also far more difficult to implement. The second topic is to be *impact forces*, that is, very large forces that act on a very short period of time. There are many practical cases where impact forces play a very important role, and a simple and efficient way to model the process becomes necessary. One of these cases is the *backlash* or *clearance* in joints. This becomes the subject of another section of this chapter. *Kinematic synthesis*, which entails the finding of the best possible dimensions for a multibody system, and *sensitivity analysis*, so useful for determining the tendencies of the optimal objective function with respect to design variations, are also dealt with in this chapter. Finally, some ways to deal with *singular positions* of multibody systems will be described.

10.1 Coulomb Friction

Coulomb, or dry modeling for friction, seems to be more accurate than viscous friction for joints with small relative velocity. Coulomb friction is also more difficult to introduce in a general purpose program because it is highly nonlinear and can involve switching between sliding and stiction conditions. A consistent consideration of the Coulomb friction model can be found in Bagci (1975) and more importantly, in Haug et al. (1986). Figure 10.1a represents the friction force dependency on relative velocity, according to the Coulomb model. In order to avoid the discontinuity at zero, some authors (Threlfall (1978) and Rooney and Deravi (1982)) have introduced more continuous dependency laws similar to the one shown in Figure 10.1b. In this section, we will be consistent with the Coulomb friction model.

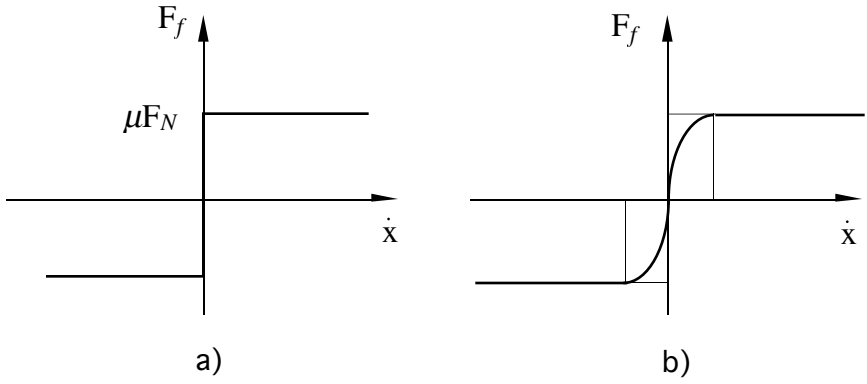

Figure 10.1. Coulomb friction models: a) standard. b) modified.

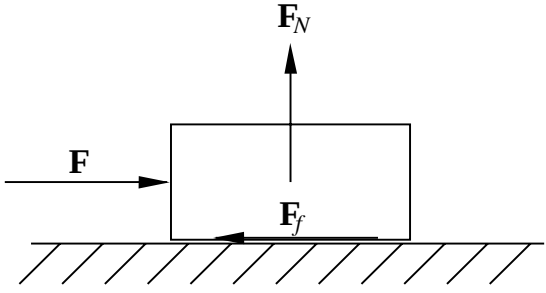

Figure 10.2. Block sliding on a plane with Coulomb friction.

10.1.1 Review of the Coulomb Friction Hypothesis

Consider a block on a flat surface as seen in Figure 10.2. The block is a body of mass m subjected to gravity forces of vertical descending direction. These forces are in equilibrium with the ground reaction force $\mathbf{F}_N$. There is some experimental evidence that if a rather small horizontal force $\mathbf{F}$ is applied to the block, no motion is obtained. This means that a horizontal reaction force $\mathbf{F}_f$ has appeared. If the external force $\mathbf{F}$ is increased little by little, it can be observed that when it reaches a particular value the block starts to move, sliding on the ground. This critical value of $\mathbf{F}$ depends on the nature of the ground and block contact surfaces and on the normal force $\mathbf{F}_N$. It also may be observed that during the relative sliding, the horizontal reaction force $\mathbf{F}_f$ (the *friction force*) depends on the normal force $\mathbf{F}_N$, but it does not depend on the velocity and/or acceleration. The mathematical model for this mechanical behavior is call *Coulomb friction* after the French scientist of the *XVIII* Century or *dry friction*, because it models reasonably well the friction forces between non-lubricated contact surfaces.

The Coulomb friction model assumes that between the block and the ground there is a normal reaction force $\mathbf{F}_N$ and a horizontal friction force $\mathbf{F}_f$.

With respect to the relative motion between the surfaces in contact, two different cases or situations are possible: *sliding* and *stiction* (or lock up)

– Sliding: $\mathbf{F}_f = \mu_d \mathbf{F}_N$ (10.1)

– Stiction: $\mathbf{F}_f \leq \mu_s \mathbf{F}_N$ (10.2)

where μ_d and μ_s are the coefficients of *dynamic* and *static* friction, respectively. Two coefficients have been introduced because there is some experimental evidence that the external force $\mathbf{F}$ necessary to start the motion is different (higher) that the force necessary to maintain the motion with constant relative velocity. Both μ_d and μ_s are constant scalar coefficients that depend on the nature of the contact surfaces (material, finishing state, etc.) but not on the external forces or motion variables. Very often both coefficients are considered as equivalent, with a single value μ.

In the *sliding* condition, the friction force $\mathbf{F}_f$ is known and the motion acceleration becomes the unknown. In the *stiction* condition, the friction force $\mathbf{F}_f$ is unknown, but there is no relative acceleration.

It is very important to set the conditions for switching between the two possible states of sliding and stiction. If the block is initially at rest, the motion will start when the external force $\mathbf{F}$ reaches the critical value, that is, maximum value for the friction force $\mathbf{F}_f$. In the stiction condition, the friction force is unknown. It shall be obtained from the horizontal equilibrium equation. The motion will start when a friction force is obtained such that

– Stiction to sliding: $\mathbf{F}_f > \mu_s \mathbf{F}_N$

If there is sliding but the external forces are changing, it is possible that a state is reached in which the relative sliding velocity changes its sign. In this case stiction will occur. The mathematical condition becomes:

– Sliding to stiction: Sliding velocity changes sign.

In summary, when there is *stiction*, the relative velocity is zero and the friction force shall be computed and checked. When it goes over its maximum value, it is necessary to switch to the *sliding* condition. In the *sliding* condition, the friction force is known, but the relative motion shall be computed and checked. When the relative velocity changes its sign, it is necessary to switch to the *stiction* condition.

The *Coulomb* friction model is quite different from *viscous* friction model, in which friction forces depend (often linearly) on velocities. Viscous dampers and the motion of a body inside a fluid environment are examples of viscous friction. Its mathematical model is simpler than the Coulomb one, mainly because there is neither force dependency on reaction forces nor switching conditions between different states governed by different sets of differential equations.

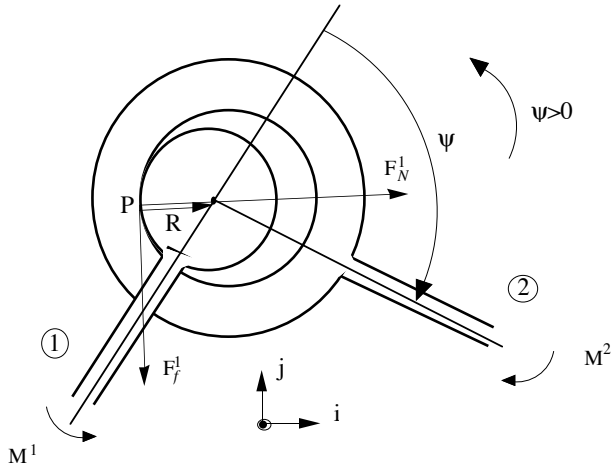

Figure 10.3. Friction forces in a planar revolute joint.

In the following sections, the Coulomb friction model will be extended for applications in complex multibody systems.

10.1.2 Coulomb Friction in Multibody Systems: Sliding Condition

In a complex multibody system, Coulomb friction may likely appear in joints where there are contacting surfaces belonging to different bodies that have relative sliding motion. The simpler and more likely to occur sliding condition will be considered first.

If there is sliding, the friction force in a joint is a known linear function of the normal reaction force in this joint. The normal reaction force can be computed from the Lagrange multipliers associated with the joint constraint equations (See Chapter 6). The corresponding equations of motion take the form (See equation (5.10)):

$$\begin{bmatrix} \mathbf{M} & \boldsymbol{\Phi}_{\mathbf{q}}^{\mathrm{T}} \\ \boldsymbol{\Phi}_{\mathbf{q}} & 0 \end{bmatrix} \begin{Bmatrix} \ddot{\mathbf{q}} \\ \boldsymbol{\lambda} \end{Bmatrix} = \begin{Bmatrix} \mathbf{Q} \\ \mathbf{c} \end{Bmatrix} \tag{10.3}$$

where the term $(\boldsymbol{\Phi}_{\mathbf{q}}^{\mathrm{T}} \boldsymbol{\lambda})$ represents the joint constraint forces. For any kind of joint, the normal forces $\mathbf{F}_N$ can be expressed as a function of the constraint forces in the form:

$$\mathbf{F}_N = \mathbf{E}(\mathbf{q}) \boldsymbol{\Phi}_{\mathbf{q}}^{\mathrm{T}} \boldsymbol{\lambda} \tag{10.4}$$

where $\mathbf{E}(\mathbf{q})$ is a term that depends on the joint geometry and sometimes on the position as well. The generalized friction forces $\mathbf{Q}_f$ are proportional to $\mathbf{F}_N$ and can be written as

$$\mathbf{Q}_f = \mu \cdot \mathbf{u}(\mathbf{q})\, \mathbf{E}(\mathbf{q})\, \boldsymbol{\Phi}_{\mathbf{q}}^{\mathrm{T}}\, \boldsymbol{\lambda} \tag{10.5}$$

where f is the friction coefficient and $\mathbf{u}(\mathbf{q})$ another function characteristic of each joint type and geometry.

Example 10.1

Consider the planar revolute joint with Coulomb friction, shown in Figure 10.3. The backlash is assumed to be small, although large enough to assure a single point of contact between the inner (1) and outer (2) circles. Force $\mathbf{F}_N^1$ is considered to be the normal contact force that body 2 exerts on body 1. This normal constraint force can be computed by solving the inverse dynamics problem, as explained in Chapter 6. Also assume that that the joint relative angle ψ has been introduced as a dependent coordinate. This will lead to an easier definition of the friction torques on the two contacting bodies.

In order to use vector expressions, the relative velocity of body 2 respect to body 1 is defined as

$$\boldsymbol{\omega}_{\mathrm{r}}^{2,1} = -\,\dot{\psi}\,\mathbf{k} \tag{i}$$

where $\mathbf{k} = \mathbf{i} \wedge \mathbf{j}$ is the unit vector normal to the plane of the mechanism. The minus sign (–) is necessary for full consistency of expression (i). The tangent friction force $\mathbf{F}_f^1$ is computed as

$$\mathbf{F}_f^1 = \mu\, \mathrm{sign}(\dot{\psi})\, \mathbf{F}_N^1 \wedge \mathbf{k} \tag{ii}$$

The friction force $\mathbf{F}_f^1$ shall be applied to body 1 at the joint center which is a basic point. It is then necessary to apply the opposite force on body 2. However, it is also necessary to apply the friction torques on both bodies. These torques can be computed by means of the following equation:

$$\mathbf{M}_f = M_f \mathbf{k} = \mathbf{F}_f^1 \wedge \frac{\mathbf{F}_N^1}{|\mathbf{F}_N^1|} R = \mu\, \mathrm{sign}(\dot{\psi})\, R\, (\mathbf{F}_N^1 \wedge \mathbf{k}) \wedge \mathbf{F}_N^1 \tag{iii}$$

The scalar value of this torque M_f is the force variable conjugated with the relative angle ψ. Therefore, it can be applied on both bodies at the same time (See Section 4.3.1).

The equations of motion with Coulomb friction become

$$\begin{bmatrix} \mathbf{M} & \boldsymbol{\Phi}_{\mathbf{q}}^{\mathrm{T}} \\ \boldsymbol{\Phi}_{\mathbf{q}} & 0 \end{bmatrix} \begin{Bmatrix} \ddot{\mathbf{q}} \\ \boldsymbol{\lambda} \end{Bmatrix} = \begin{Bmatrix} \mathbf{Q} + \mathbf{Q}_f(\boldsymbol{\lambda}) \\ \mathbf{c} \end{Bmatrix} \tag{10.6}$$

It may be seen that the vector of Lagrange multipliers $\boldsymbol{\lambda}$ appears on both sides of the equation. Therefore it must be solved iteratively. A possible algorithm, based on fixed point iteration, is the following one:

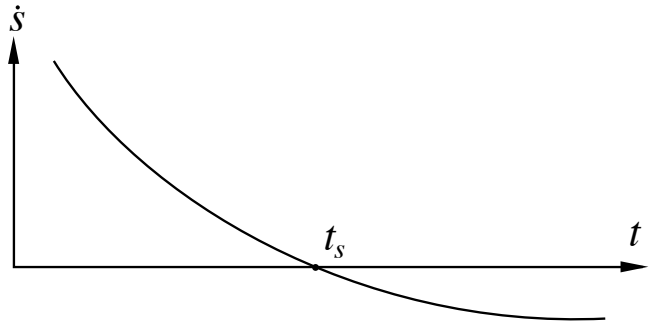

Figure 10.4. Change of sign of sliding velocity.

Algorithm 10-1

1. Estimate $\boldsymbol{\lambda}^0$. Compute $\mathbf{Q}_f(\boldsymbol{\lambda}^0)$. Set $i = 0$
2. Calculate $\boldsymbol{\lambda}^{i+1}$ from (10.6) adjusted for fixed point iteration

$$\begin{bmatrix} \mathbf{M} & \boldsymbol{\Phi}_{\mathbf{q}}^{\mathrm{T}} \\ \boldsymbol{\Phi}_{\mathbf{q}} & 0 \end{bmatrix} \begin{Bmatrix} \ddot{\mathbf{q}} \\ \boldsymbol{\lambda}^{i+1} \end{Bmatrix} = \begin{Bmatrix} \mathbf{Q} + \mathbf{Q}_f(\boldsymbol{\lambda}^i) \\ \mathbf{c} \end{Bmatrix}$$

3. If abs($\boldsymbol{\lambda}^{i+1}$–$\boldsymbol{\lambda}^i$) < *tolerance*, stop. Otherwise, go to step 4.
4. Set $\boldsymbol{\lambda}^{i+1}$=$\boldsymbol{\lambda}^i$, i=i+1, and go to step 2.

Remember that the friction force $\mathbf{F}_f$, which may be obtained from an equation analogous to (10.5), needs be checked in relation with $\mathbf{F}_N$ in order to see if the assumed *sliding* condition remains valid.

10.1.3 Coulomb Friction in Multibody Systems: Stiction Condition.

The sliding relative velocity must be monitored during the sliding condition. At time t_s, if a change in the relative velocity sign is detected (See Figure 10.4), the joint becomes locked, and it is then necessary to switch to the stiction condition.

The joint lock-up can be represented mathematically by a new constraint equation. In a revolute joint, for instance, the relative angle must be kept constant. The stiction constraint equation can be written in the general form:

$$\boldsymbol{\Phi}^{\mathrm{r}} = 0 \tag{10.7}$$

This new equation is appended to the remaining constraints, leading to a system of dynamic equations similar to (10.6)

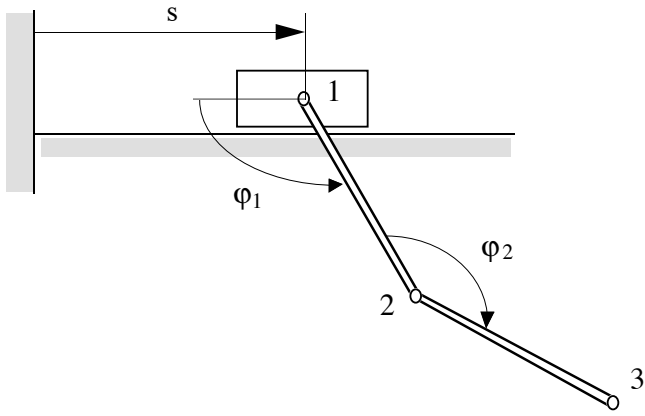

Figure 10.5. Planar mechanism with Coulomb friction in the joints.

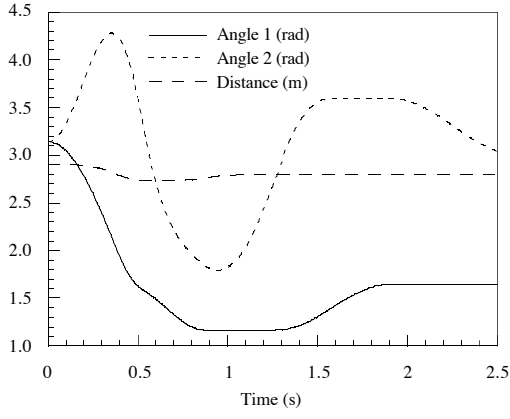

Figure 10.6. Time variation of the joint coordinates.

$$\begin{bmatrix} \mathbf{M} & \boldsymbol{\Phi}_{\mathbf{q}}^{\mathrm{T}} & \boldsymbol{\Phi}_{\mathbf{q}}^{\mathrm{rT}} \\ \boldsymbol{\Phi}_{\mathbf{q}} & 0 & 0 \\ \boldsymbol{\Phi}_{\mathbf{q}}^{\mathrm{r}} & 0 & 0 \end{bmatrix} \begin{Bmatrix} \ddot{\mathbf{q}} \\ \boldsymbol{\lambda} \\ \boldsymbol{\lambda}^{\mathrm{r}} \end{Bmatrix} = \begin{Bmatrix} \mathbf{Q} \\ \mathbf{c} \\ \mathbf{c}^{\mathrm{r}} \end{Bmatrix} \tag{10.8}$$

At this point, the stiction force $\mathbf{F}_f$ is to be computed and monitored. It can be computed from the force associated with the stiction constraint (10.7) in the form:

$$\mathbf{F}_f = \mathbf{D}(\mathbf{q})\,\boldsymbol{\Phi}_{\mathbf{q}}^{\mathrm{rT}}\,\boldsymbol{\lambda}^{\mathrm{r}} \tag{10.9}$$

where $\mathbf{D}(\mathbf{q})$ is again a term that depends on the joint type, geometry, and position. This friction or stiction force shall be checked so as to be sure that it is below its maximum value. This value is the normal force multiplied by the coefficient of friction. When it is found that

$$\mathbf{F}_f > \mu\,\mathbf{F}_N \tag{10.10}$$

it is necessary to switch to the sliding condition, releasing the previously added constraint equation (10.7).

The mathematical model for the Coulomb friction is not easy to implement in general purpose codes, even for the simplest cases. It is not currently implemented with generality in any commercial simulation package to the authors' knowledge. The difficulties stem from the switching between sliding and stiction states involving a change in the number of the system degrees of freedom and the need to iterate, in the sliding state, for each acceleration evaluation with equation (10.6).

Example 10.2

Figure 10.5 shows a planar multibody system consisting on a double pendulum joined to the fixed element through a prismatic joint that allows a horizontal translation. The physical characteristics of the problem are:

$L_{12} = L_{23} = 1$ m.
$m_1 = m_2 = 10$ kg.
$I_2 = I_3 = 0$
$\mu_P = 0{,}25$ $\mu_1 = 0{,}14$ $\mu_2 = 0{,}11$

where μ_P is the friction coefficient at the prismatic joint, and μ_1, and μ_2 are the friction coefficient at the revolute joints 1 and 2. The pendulum starts moving from the horizontal position and falls under gravity effects. Figure 10.6 shows the time history of the three relative coordinates. It may be seen how these curves remain flat during some time intervals. This means that during those time intervals the corresponding joint is locked due to friction.

10.2 Impacts and Collisions

Impacts are due to large impulsive forces, acting over infinitesimal periods of time. The mathematical representation of impacts can be done with the *unit impulse* or *Dirac delta function* $\delta(t–a)$. This function can be seen as the limit of a rectangle function of unit area centered at time a, when the width ε tends to zero as can be seen in Figure 10.7.

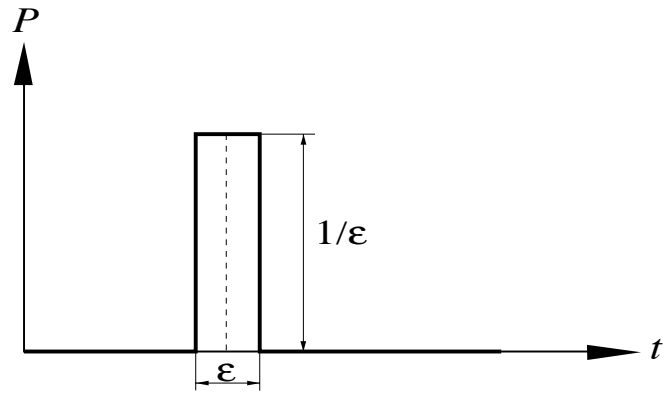

Figure 10.7. Rectangular function of unit area.

As ε goes to zero, the function value becomes infinite, but the area under the function remains equal to the unit value. The product of the Dirac delta function by an arbitrary function *f(t)* satisfies the following property:

$$\int_{-\infty}^{\infty} f(t)\ \delta(t-a)\ dt = f(a) \tag{10.11}$$

that is used sometimes as an alternative definition for function $\delta(t-a)$.

A general discussion on impact forces in multibody systems was presented by Haug et al. (1986).

10.2.1 Known Impact Forces

It is customary in mechanics to compute the effect of impacts on bodies assuming that during the impact all the remaining finite forces can be neglected. It is also assumed that the system position does not change, because the impact time is very small. As with the Dirac function, the equations of motion under impulsive forces can be considered in an integral form. For instance, the equations of motion (10.3) with known impulse forces $\mathbf{Q}^{\mathrm{i}}$ acting at time t_i become

$$\begin{bmatrix} \mathbf{M} & \boldsymbol{\Phi}_{\mathbf{q}}^{\mathrm{T}} \\ \boldsymbol{\Phi}_{\mathbf{q}} & 0 \end{bmatrix} \begin{Bmatrix} \ddot{\mathbf{q}} \\ \boldsymbol{\lambda} \end{Bmatrix} = \begin{Bmatrix} \mathbf{Q} + \mathbf{Q}^{\mathrm{i}} \\ \mathbf{c} \end{Bmatrix} \tag{10.12}$$

Integrating from time t_i^- to t_i^+:

$$\int_{t_i^-}^{t_i^+} (\mathbf{M}\ddot{\mathbf{q}} + \boldsymbol{\Phi}_{\mathbf{q}}^{\mathrm{T}}\boldsymbol{\lambda})\ dt = \int_{t_i^-}^{t_i^+} (\mathbf{Q} + \mathbf{Q}^{\mathrm{i}})\ dt \tag{10.13}$$

$$\int_{t_i^-}^{t_i^+} \boldsymbol{\Phi}_{\mathbf{q}} \ddot{\mathbf{q}}\, dt = \int_{t_i^-}^{t_i^+} \mathbf{c}\, dt \tag{10.14}$$

Using incremental notation, one obtains:

$$\mathbf{M}\ \Delta\dot{\mathbf{q}} + \boldsymbol{\Phi}_{\mathbf{q}}^{\mathrm{T}}\, \boldsymbol{\lambda}_{\mathrm{p}} = \mathbf{P}^{\mathrm{i}} \tag{10.15}$$

$$\boldsymbol{\Phi}_{\mathbf{q}}\ \Delta\dot{\mathbf{q}} = 0 \tag{10.16}$$

where $\boldsymbol{\lambda}_{\mathrm{p}}$ are the Lagrange multipliers that are related to the internal impact forces (impact reactions), and $\mathbf{P}^{\mathrm{i}}$ is the *integral effect* of the impact forces. Equation (10.15) represents the *conservation of momentum*, and equation (10.16) states that the velocity increment shall fulfill the homogeneous velocity constraint equations. In equation (10.15), $\mathbf{P}^{\mathrm{i}}$ is

$$\mathbf{P}^{\mathrm{i}} = \int_{t_i^-}^{t_i^+} \mathbf{Q}^{\mathrm{i}}\, dt \tag{10.17}$$

Writing equations (10.15) and (10.16) jointly in matrix form, one can obtain

$$\begin{bmatrix} \mathbf{M} & \boldsymbol{\Phi}_{\mathbf{q}}^{\mathrm{T}} \\ \boldsymbol{\Phi}_{\mathbf{q}} & 0 \end{bmatrix} \begin{Bmatrix} \Delta\dot{\mathbf{q}} \\ \boldsymbol{\lambda}_{\mathrm{p}} \end{Bmatrix} = \begin{Bmatrix} \mathbf{P}^{\mathrm{i}} \\ 0 \end{Bmatrix} \tag{10.18}$$

It may be seen from equation (10.18), that the mechanical effect of a known impulse is an instantaneous increment in the system velocities $\dot{\mathbf{q}}$. If the impact forces $\mathbf{P}^{\mathrm{i}}$ are known, the dynamic simulation can proceed according to the following algorithm:

Algorithm 10-2

1. Integrate the equations of motion from $t = 0$ to $t = t_i$ using the equations

$$\begin{bmatrix} \mathbf{M} & \boldsymbol{\Phi}_{\mathbf{q}}^{\mathrm{T}} \\ \boldsymbol{\Phi}_{\mathbf{q}} & 0 \end{bmatrix} \begin{Bmatrix} \ddot{\mathbf{q}} \\ \boldsymbol{\lambda} \end{Bmatrix} = \begin{Bmatrix} \mathbf{Q} \\ \mathbf{c} \end{Bmatrix} \tag{10.19}$$

2. At $t = t_i$, during the actuation of the impact force, use the equation

$$\begin{bmatrix} \mathbf{M} & \boldsymbol{\Phi}_{\mathbf{q}}^{\mathrm{T}} \\ \boldsymbol{\Phi}_{\mathbf{q}} & 0 \end{bmatrix} \begin{Bmatrix} \Delta\dot{\mathbf{q}} \\ \boldsymbol{\lambda}_{\mathrm{p}} \end{Bmatrix} = \begin{Bmatrix} \mathbf{P}^{\mathrm{i}} \\ 0 \end{Bmatrix} \tag{10.20}$$

to compute jump discontinuity in velocities and find the velocities after the impact as

$$\dot{\mathbf{q}}(t_i^+) = \dot{\mathbf{q}}(t_i^-) + \Delta\dot{\mathbf{q}} \tag{10.21}$$

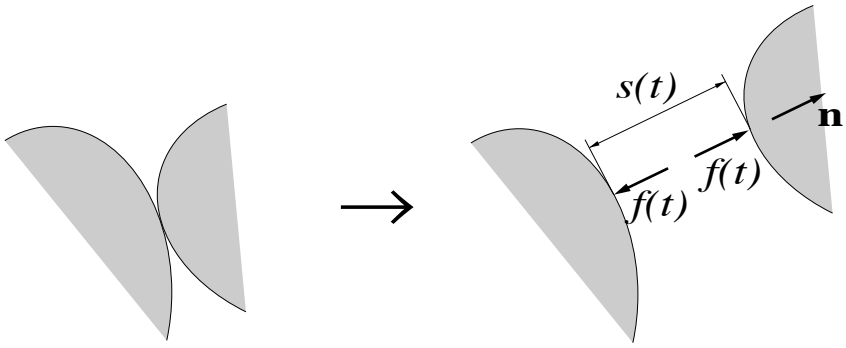

Figure 10.8. Impact between two bodies.

3. Use the new velocities $\dot{\mathbf{q}}$ resulting from (10.21) to restart the numerical integration.

10.2.2 Impacts Between Bodies

When two bodies impact against each other, an unknown impulsive force acts between them. In this case, equation (10.20) cannot be used because the impact $\mathbf{P}^{\mathrm{i}}$ is not known. According to the physical characteristics of the bodies, one normally knows if the impact is perfectly *elastic* (because there is a perfect rebound), perfectly *plastic* (where there is no rebound at all), or something in between. One can use this information to compute the velocities after the impact.

In Figure 10.8, two bodies can be seen impacting and rebounding. Vector **n** is a unit vector normal to the body surfaces in the contact point; s is the distance between the contact points, and $\mathbf{f}(t)$ is the impact force.

The virtual work produced by $\boldsymbol{f}(t)$ is

$$\delta W = f\ \delta s = f\ \left(\frac{\partial s}{\partial \mathbf{q}}\right)^{\mathrm{T}} \delta \mathbf{q} \tag{10.22}$$

and the generalized impulse $\mathbf{P}^{\mathrm{i}}$ is given by the integral of the generalized force between t_i^- and t_i^+ leading to

$$\mathbf{P}^{\mathrm{i}} = \frac{\partial s}{\partial \mathbf{q}}\, p \tag{10.23}$$

where

$$p = \int_{t_i^-}^{t_i^+} f(t)\, dt \tag{10.24}$$

Since the magnitude p of the impact is unknown, the additional equation that arises from the impact characteristics of the bodies is needed. From experimental

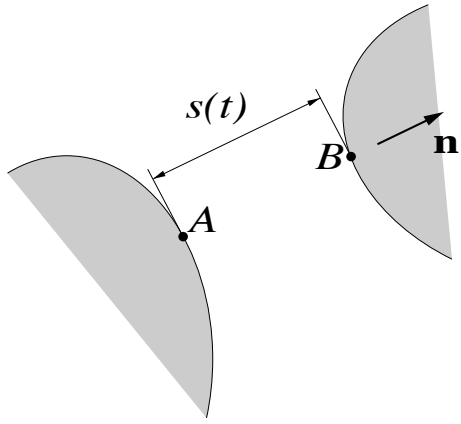

Figure 10.9. Points in contact during the impact.

testing, it is known that the normal relative velocities of the contact points before and after the impact are related by

$$\dot{s}(t_i^+) = -\, e\, \dot{s}(t_i^-) \tag{10.25}$$

where e is called the *coefficient of restitution* or Newton's coefficient. If the impact is perfectly *elastic* (e=1), the normal relative velocity changes its sign but keeps the magnitude. On the other hand, if the impact is perfectly *plastic* (e=0), there is no rebound or normal relative velocity after the impact. Notice that this formulation assumes that there is no friction or tangent impact forces. Impact with friction is a very specialized and difficult subject and will not be considered here.

Next the equations for the impact will be developed. Using the chain rule of differentiation for the normal relative velocity,

$$\dot{s} = \left(\frac{\partial s}{\partial \mathbf{q}}\right)^{\mathrm{T}} \dot{\mathbf{q}} \tag{10.26}$$

Substituting this in equation (10.25) yields

$$\left(\frac{\partial s}{\partial \mathbf{q}}\right)^{\mathrm{T}} \dot{\mathbf{q}}(t_i^+) = -\, e \left(\frac{\partial s}{\partial \mathbf{q}}\right)^{\mathrm{T}} \dot{\mathbf{q}}(t_i^-) \tag{10.27}$$

Subtracting $\dfrac{\partial s}{\partial \mathbf{q}}\, \dot{\mathbf{q}}(t_i^-)$ from both sides of equation (10.27), one obtains

$$\left(\frac{\partial s}{\partial \mathbf{q}}\right)^{\mathrm{T}} \Delta \dot{\mathbf{q}} = -\,(1+e) \left(\frac{\partial s}{\partial \mathbf{q}}\right)^{\mathrm{T}} \dot{\mathbf{q}}(t_i^-) \tag{10.28}$$

This last equation can be written together with the impulse equations (10.18), yielding

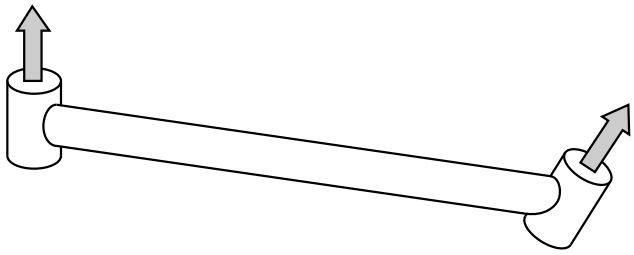

Figure 10.10. Element defined with two points and two unit vectors.

$$\begin{bmatrix} \mathbf{M} & \boldsymbol{\Phi}_{\mathbf{q}}^{\mathrm{T}} & \dfrac{\partial s}{\partial \mathbf{q}} \\ \boldsymbol{\Phi}_{\mathbf{q}} & 0 & 0 \\ \left(\dfrac{\partial s}{\partial \mathbf{q}}\right)^{\mathrm{T}} & 0 & 0 \end{bmatrix} \begin{Bmatrix} \Delta\dot{\mathbf{q}} \\ \boldsymbol{\lambda}_{\mathrm{p}} \\ -p \end{Bmatrix} = \begin{Bmatrix} 0 \\ 0 \\ -(1+e)\left(\dfrac{\partial s}{\partial \mathbf{q}}\right)^{\mathrm{T}} \dot{\mathbf{q}}(t_i^-) \end{Bmatrix} \tag{10.29}$$

The derivative $\partial s/\partial \mathbf{q}$ needs to be computed next. The two points that will be in contact during the impact are called A and B, as can be seen in Figure 10.9.

According to the expressions developed in Chapter 4, the position vectors $\mathbf{r}_{\mathrm{A}}$ and $\mathbf{r}_{\mathrm{B}}$ can be written as linear combinations of the elements of the dependent coordinates vector $\mathbf{q}$ (See equations (4.50) or (4.90)) in the form

$$\mathbf{r}_{\mathrm{A}} = \mathbf{C}_{\mathrm{A}}\, \mathbf{q} \tag{10.30}$$

$$\mathbf{r}_{\mathrm{B}} = \mathbf{C}_{\mathrm{B}}\, \mathbf{q} \tag{10.31}$$

For an element defined with two points and two vectors as the one in figure 10.10, $\mathbf{C}_{\mathrm{A}}$ and $\mathbf{C}_{\mathrm{B}}$ are constant matrices.

Thus, the distance s can be expressed as

$$s^2 = \left(\mathbf{r}_{\mathrm{A}} - \mathbf{r}_{\mathrm{B}}\right)^{\mathrm{T}} \left(\mathbf{r}_{\mathrm{A}} - \mathbf{r}_{\mathrm{B}}\right) \tag{10.32}$$

Differentiating with respect to $\mathbf{q}$ yields

$$\frac{\partial s}{\partial \mathbf{q}} = \frac{\partial\left(\mathbf{r}_{\mathrm{A}} - \mathbf{r}_{\mathrm{B}}\right)^{\mathrm{T}}}{\partial \mathbf{q}} \frac{\mathbf{r}_{\mathrm{A}} - \mathbf{r}_{\mathrm{B}}}{s} = (\mathbf{C}_{\mathrm{A}}^{\mathrm{T}} - \mathbf{C}_{\mathrm{B}}^{\mathrm{T}})\, \mathbf{n} = \mathbf{C}_{\mathrm{AB}}^{\mathrm{T}}\, \mathbf{n} \tag{10.33}$$

Substituting this result in equation (10.29), one obtains

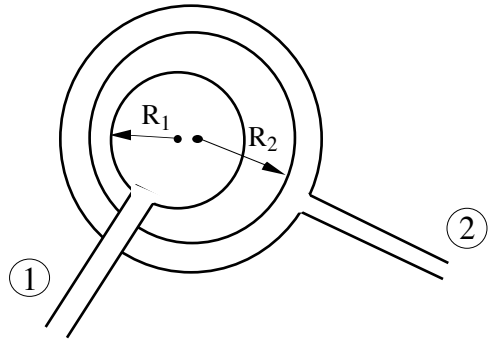

Figure 10.11. Planar revolute joint with backlash.

$$\begin{bmatrix} \mathbf{M} & \boldsymbol{\Phi}_{\mathbf{q}}^{\mathrm{T}} & \mathbf{C}_{\mathrm{AB}}\,\mathbf{n}^{\mathrm{T}} \\ \boldsymbol{\Phi}_{\mathbf{q}} & 0 & 0 \\ \mathbf{C}_{\mathrm{AB}}^{\mathrm{T}}\,\mathbf{n} & 0 & 0 \end{bmatrix} \begin{Bmatrix} \Delta\dot{\mathbf{q}} \\ \boldsymbol{\lambda}_{\mathrm{p}} \\ -p \end{Bmatrix} = \begin{Bmatrix} 0 \\ 0 \\ -(1+e)\,\mathbf{C}_{\mathrm{AB}}^{\mathrm{T}}\,\mathbf{n}\;\dot{\mathbf{q}}(t_i^-) \end{Bmatrix} \tag{10.34}$$

This system of linear equations allows the computation of all the unknown parameters. The new velocities after the impact are

$$\dot{\mathbf{q}}(t_i^+) = \dot{\mathbf{q}}(t_i^-) + \Delta\dot{\mathbf{q}} \tag{10.35}$$

and one also obtains the magnitude of the impact p and the internal reaction or constraint impacts ($\boldsymbol{\Phi}_{\mathbf{q}}^{\mathrm{T}}\,\boldsymbol{\lambda}_{\mathrm{p}}$).

Remark. Equation (10.34) can be modified so as to eliminate the internal impact forces by expressing it in terms of the increment of the independent velocities with the use of the matrix $\mathbf{R}$ introduced in Section 3.5. After some algebraic manipulations, one can obtain

$$\begin{bmatrix} \mathbf{R}^{\mathrm{T}}\,\mathbf{M}\,\mathbf{R} & \mathbf{R}^{\mathrm{T}}\,\mathbf{n}^{\mathrm{T}}\,\mathbf{C}_{\mathrm{AB}} \\ \mathbf{C}_{\mathrm{AB}}^{\mathrm{T}}\,\mathbf{n}\,\mathbf{R} & 0 \end{bmatrix} \begin{Bmatrix} \Delta\dot{\mathbf{z}} \\ -p \end{Bmatrix} = \begin{Bmatrix} 0 \\ -(1+e)\,\mathbf{C}_{\mathrm{AB}}^{\mathrm{T}}\,\mathbf{n}\;\dot{\mathbf{q}}(t_i^-) \end{Bmatrix} \tag{10.36}$$

This concludes the formulation of impacts between bodies.

10.3 Backlash

The problem of *backlash* or existing *clearances* in joints is an important practical problem in many applications that may produce noise, vibrations, severe damage and other difficulties in normal operation of real multibody systems. Some results on this subject for complex mechanical systems can be found in Dubowsky et al. (1987).

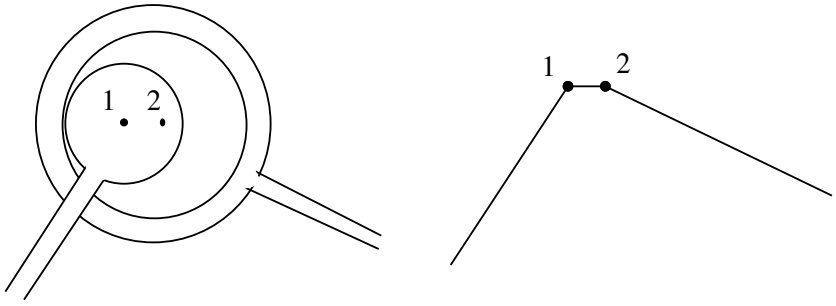

Figure 10.12. Contact condition in a revolute joint with backlash.

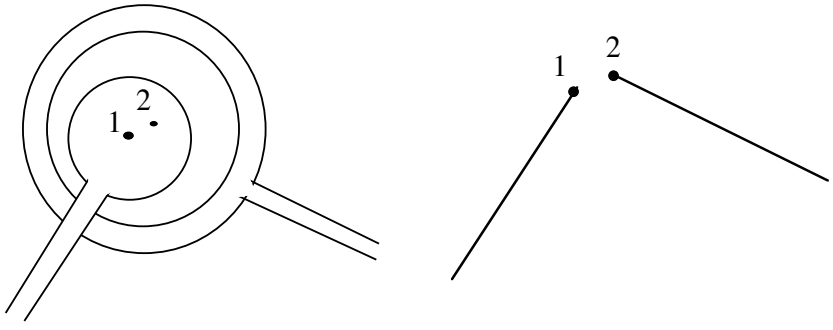

Figure 10.13. Non-contact condition in a revolute joint with backlash.

Backlash is a difficult problem to model because it depends on poorly known data, as for instance the clearance magnitude itself. Backlash is also a problem that strongly depends on the particular geometry of the joint. In a 3-D revolute joint with backlash, there are many possible ways to set the physical contact between the inner and outer cylinders, and a general formulation for backlash largely exceeds the aims and scope of this section. This text will be limited to introducing some backlash concepts using the planar revolute and prismatic joints.

10.3.1 Planar Revolute Joint

Figure 10.11 shows a planar revolute joint where the backlash has been made very large in order to make it clearly visible. This joint is materialized by two circles, the inner of radius R_1 and belonging to body 1, and the outer of radius R_2 and belonging to body 2. One can assume that points 1 and 2 are the centers of the two circles. In this case, the revolute joint shall be considered with two points and not with a single shared point, as in Chapter 2.

It is easy to see that there are two possible scenarios:

a) *The two circles are in contact*. The mathematical condition for this case is that the distance between the circle centers should be equal to the difference of radius (clearance):

$$(x_1 - x_2)^2 + (y_1 - y_2)^2 - (R_2 - R_1)^2 = 0 \tag{10.37}$$

As long as the circles are in contact, the centers move as if they were connected by a rigid bar 1-2, of length $d_{12}^2 = (R_2 - R_1)^2$. Thus the joint can be replaced by an equivalent mechanism with an additional bar as indicated in Figure 10.12.

b) *The two circles are not in contact*. In this case, elements 1 and 2 move independently, and there is not any mathematical constraint equation between them as may be seen in Figure 10.13. The following inequality must be fulfilled:

$$(x_1 - x_2)^2 + (y_1 - y_2)^2 - (R_2 - R_1)^2 < 0 \tag{10.38}$$

It remains to explain when the joint switches from condition (a) to condition (b), and vice versa.

Assume that the system is under condition (a). In this case, the constraint equation (10.37) must be added to the system constraint equations $\mathbf{\Phi}(\mathbf{q})=\mathbf{0}$ as an additional dynamic constraint $\phi_{m+1}(\mathbf{q})=0$. If equation (10.37) is added to the dynamics through a Lagrange multiplier λ_{m+1}, this multiplier represents the axial force exerted by the fictitious bar that joins the centers of the circles. This force also represents the contact force between both circles. The value of λ_{m+1} may only represent a tensional force, or, in other words, the fictitious bar can avoid a separation between points 1 and 2, but it is not able to actuate if the points tend to join each other. Therefore, the value of λ_{m+1} shall be checked in each integration step to make sure that it is positive. If so, the joint is under condition (a), and this value remains positive. If λ_{m+1} changes its sign, the constraint equation (10.37) must be removed and one should switch to case (b).

Consider now that the system is under condition (b).

In this case, bodies 1 and 2 move independently; consequently, the equations of motion are integrated without any constraint equation for the joint where the backlash is located. It is only necessary to check the inequality (10.38).

If condition (10.38) is not fulfilled, a contact between the two circles occurs. This represents a real impact between bodies 1 and 2. We can assume that because lubricant in the joint and small relative velocities, the impact is perfectly plastic with no rebound. In order to solve for the new dependent velocities after the impact $\dot{\mathbf{q}}(t^+) = \dot{\mathbf{q}}(t^-) + \Delta\dot{\mathbf{q}}$, one can use equation (10.34) by taking into account that points A and B are points 1 and 2, and thus matrices $\mathbf{C}_A$ and $\mathbf{C}_B$ can be taken as unit matrices. Equation (10.34) also provides the impact force and the remaining internal impact reaction forces. At time (t^+), the numerical integration is restarted including equation (10.37), because one is now in case (a). If in addition to backlash there is also Coulomb friction in the joint, the formula-

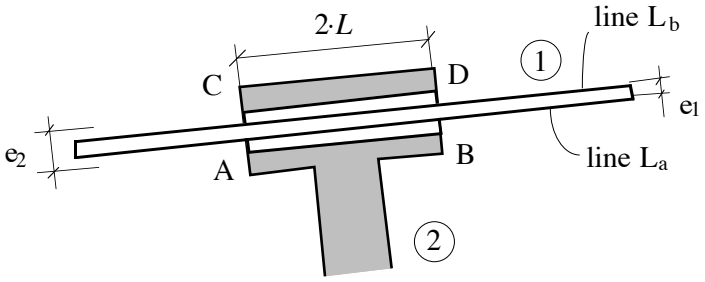

Figure 10.14. Planar prismatic joint with backlash.

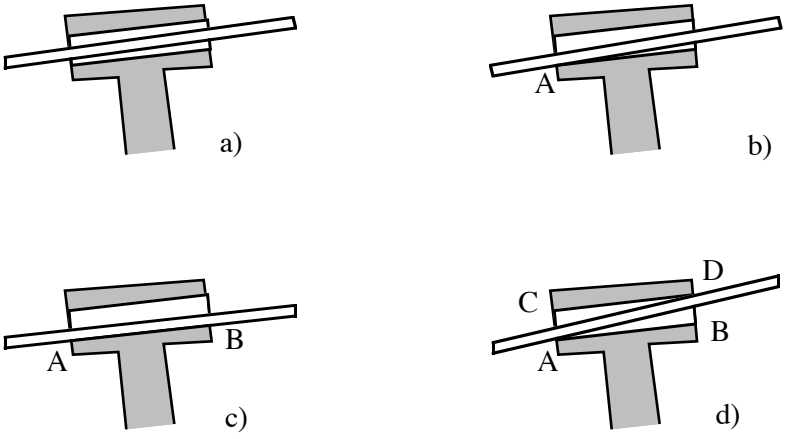

Figure 10.15. Four contact possibilities for a prismatic joint with backlash.

tion becomes more involved and will not be discussed here. It is necessary again to watch the normal force between the circles in order to check the contact condition, but now there is also a tangent friction force that can be introduced as an external force. As this external force changes the value of the normal force, it is necessary to iterate inside each integration step, as explained in Section 10.1.

10.3.2 Planar Prismatic Joint

The formulation of backlash for this kind of joint is more complicated than that for the revolute one. Figure 10.14 illustrates a possible geometry for a prismatic joint with backlash.

The possible scenarios for the backlash in a prismatic joint are illustrated in Figure 10.15, and consist of:

a) No contact (Figure 10.15a).
b) Contact on a single point (Figure 10.15b).

c) Contact on two points on the same side (Figure 10.15c).
d) Contact on two opposed points (Figure 10.15d).

Consider four points (A, B, C, and D) defined on element 2 and two lines (*L* and *L'*) defined on element 1. The equations corresponding to segments *L* and *L'* can be expressed as a function of the dependent coordinates of body 1 ($\mathbf{q}^1$) and the coordinates of points A, B, C, and D, which may be expressed as functions of the dependent coordinates of body 2 ($\mathbf{q}^2$)

Segment L: $$y - m(\mathbf{q}^1)x - Y(\mathbf{q}^1) = 0 \tag{10.39}$$

Segment L': $$y - m'(\mathbf{q}^1)x - Y'(\mathbf{q}^1) = 0 \tag{10.40}$$

Point A: $$x_A = a_x(\mathbf{q}^2) \tag{10.41}$$

$$y_A = a_y(\mathbf{q}^2) \tag{10.42}$$

Point B: $$x_B = b_x(\mathbf{q}^2) \tag{10.43}$$

$$y_B = b_y(\mathbf{q}^2) \tag{10.44}$$

Point C: $$x_C = c_x(\mathbf{q}^2) \tag{10.45}$$

$$y_C = c_y(\mathbf{q}^2) \tag{10.46}$$

Point D: $$x_D = d_x(\mathbf{q}^2) \tag{10.47}$$

$$y_D = d_y(\mathbf{q}^2) \tag{10.48}$$

where m, m', Y, Y', a_x, a_y, b_x, b_y, c_x, c_y, d_x, d_y are known functions of the dependent coordinates vector of the corresponding element.

Using these expressions, it is possible to set the constraint equations corresponding to the four cases in Figure 10.15. This is done in the following way:

a) No constraint equations are necessary.
b) Point A shall be on line *L*. Substituting equation (10.41) on equation (10.39):

$$a_y(\mathbf{q}^2) - m(\mathbf{q}^1) \cdot a_x(\mathbf{q}^2) - Y(\mathbf{q}^1) = 0 \tag{10.49}$$

c) Points A and B shall be on line *L*. The corresponding equations are:

$$a_y(\mathbf{q}^2) - m(\mathbf{q}^1) \cdot a_x(\mathbf{q}^2) - Y(\mathbf{q}^1) = 0 \tag{10.50}$$

$$b_y(\mathbf{q}^2) - m(\mathbf{q}^1) \cdot b_x(\mathbf{q}^2) - Y(\mathbf{q}^1) = 0 \tag{10.51}$$

d) Points A and D shall be on lines L and L', respectively. The constraint equations are

$$a_y(\mathbf{q}^2) - m(\mathbf{q}^1) \cdot a_x(\mathbf{q}^2) - Y(\mathbf{q}^1) = 0 \tag{10.52}$$

$$d_y(\mathbf{q}^2) - m'(\mathbf{q}^1) \cdot d_x(\mathbf{q}^2) - Y'(\mathbf{q}^1) = 0 \tag{10.53}$$

Once again, the conditions for switching from one case to a different one depend on the dynamics. In particular they depend on the constraint forces that correspond to the constraint equations (10.49)-(10.53). If the constraint equations are introduced into the dynamics through the Lagrange multipliers or augmented Lagrangian formulations (See Chapter 5), the multipliers directly represent the contact forces (it will be assumed again that there is no friction in this case). Contrary to the fictitious bars in revolute joints, in direct contact only compressive contact forces are allowed. If the sign of a contact force changes, the corresponding constraint must be removed.

When the joint is in either case (a) or (b), there is also the possibility of going into an impact condition. This condition can be detected by checking the position of point D with respect to segment L'. If an impact is detected, equation (10.34) will have to be applied to obtain a new velocity distribution. The numerical integration will have to be restarted again with the new constrain equation included.

Backlash may have additional difficulties because of the extremely small space and time scales in which losses of contact, impacts, and so forth take place. It is necessary, therefore, to use very small time steps and some interpolation techniques to capture very precisely the time of occurrence of those events. When there are many joints with backlash within the same system, the computations become exceedingly expensive.

10.4 Kinematic Synthesis

The method presented in this section is a contribution coming from Alvarez and Jiménez (1992).

In the previous chapters and sections, the most important formulations for the kinematic and dynamic *analysis* of multibody systems have been presented. In all these problems, it has been assumed that the system was *perfectly known* either because it is an existing system or it has been previously designed. When wishing to design a new system which must comply with certain specifications and only analysis tools available, one must proceed in a iterative *trial-and-error* manner by means of *re-analysis*. A preliminary design is carried out and the system is analyzed. Once the results of the analysis have been obtained and are not entirely satisfactory, the design is then modified. Another analysis is performed, and the same mode is proceeded with until the desired effect is attained.

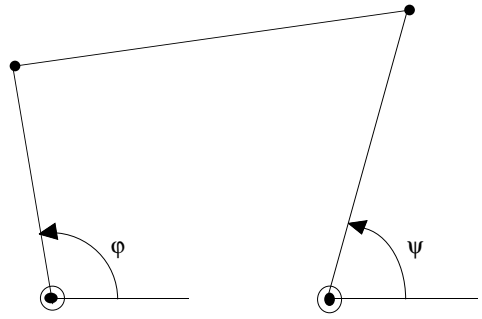

Figure 10.16. Function generation kinematic synthesis.

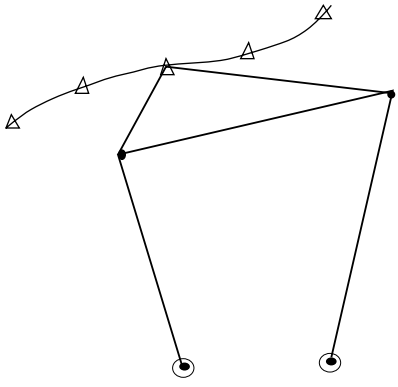

Figure 10.17. Path generation kinematic synthesis.

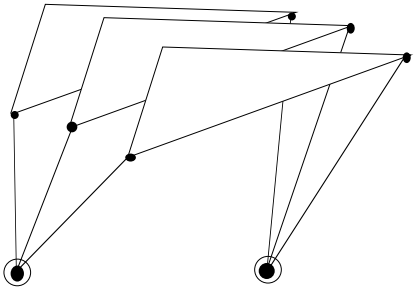

Figure 10.18. Rigid body guidance kinematic synthesis.

This *trial-and-error* process may be slow and quite dependent upon the experience of the designer.

Synthesis or *design* methods help overcome this difficulty, or at least lessen it. These methods lead directly without the intervention of an analyst, to a design which complies with the given specifications or which is the best one available from a certain point of view. The design of a multibody system can also be carried out from a more general perspective by taking dynamic factors into account. Two different problems will be studied: pure kinematic design, also called *kinematic synthesis*, and the more general *sensitivity analysis* for optimal dynamic problems.

Kinematic synthesis of mechanisms is mainly a geometric problem about which much has been written in the last half of the past century and in the first half of the present one (Angeles (1982), Erdman and Sandor (1978), and Suh and Radcliffe (1978)). During this time, many methods were developed. The majority of these methods were focused on the planar four-bar mechanism, with most of them graphic and containing a notable amount of ingenuity and originality.

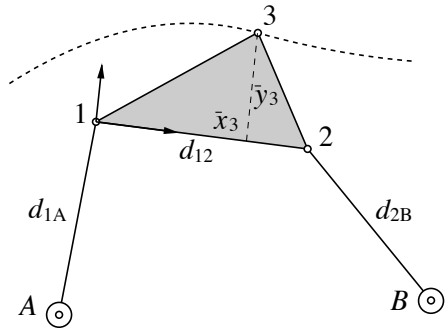

Figure 10.19. Path generated by a point of the coupling bar.

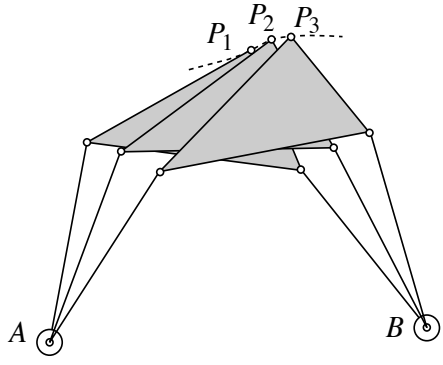

Figure 10.20. Design points for a path generation synthesis.

The traditional problems of *dimensional* synthesis are grouped together in three families: *function generation* synthesis, *path generation* synthesis, and *rigid body guidance* synthesis. An example of the function generation problem is shown in Figure 10.16. The purpose of this type of synthesis is to achieve an output angle ψ that is as close as possible to the desired nominal angle φ.

Figure 10.17 graphically illustrates a path generation problem. This basically consists of designing a four-bar mechanism so that a specific point of the coupler draws a trajectory that passes through a series of predefined points, or, at least, comes as close to them as possible.

The rigid body guidance problem can finally be seen in Figure 10.18. In this case, the design requirement is to obtain a four-bar mechanism in which a certain specific reference frame linked to the coupler passes through (or comes as close as possible to) a series of pre-established positions.

Graphic methods of kinematic synthesis are limited to simple mechanisms. They tend to be too specific and at times difficult to use. In recent years, more general programs for *optimal synthesis* have been developed. They are applicable

to many different types of planar and three-dimensional multibody systems and include many different design conditions or specifications. Normally, these methods are based on numerical methods for optimization that seek the optimal solution with a minimum degree of error.

In this section, a simple and general numerical method will be described that is an improved version of the method presented by Avilés et al. (1985) for the optimal kinematic synthesis of linkages. Although this method will be described with a path generation problem for a four-bar example, it may be easily generalized for nearly any planar or three-dimensional linkage.

In order to carry out the optimum design of a multibody system for a defined set of design specifications, three steps shall be considered:

a) Choose the multibody system *topology*
b) Select the *design variables*
c) Define and minimize the *objective function*

Two kinds of constraint equations will be described: *geometric* constraints and *functional* constraints. The geometric constraints come from the multibody system topology (step (a)), and are the constraints that have been considered in Chapters 2 and 3 of this book. The functional constraints come from the specific design requirements that the multibody systems must fulfill.

Example 10.3

As a particular example, one can consider the path generated by point 3 belonging to the coupler of the four-bar mechanism in Figure 10.19.

Consider that points A and B cannot be moved; thus the design variables are the elements of the following vector:

$$\mathbf{b}^{\mathrm{T}} = \{d_{1\mathrm{A}},\ d_{12},\ d_{2\mathrm{B}},\ \overline{x}_3,\ \overline{y}_3\} \tag{i}$$

The vector of dependent coordinates is

$$\mathbf{q}^{\mathrm{T}} = \{x_1,\ y_1,\ x_2,\ y_2,\ x_3,\ y_3\} \tag{ii}$$

In this example, the geometric constraints are the constraints that correspond to the particular system being considered. In this case, the system is a four-bar mechanism with three points in the coupler, whose geometric constraints are:

$$\phi_1 \equiv (x_1 - x_{\mathrm{A}})^2 + (y_1 - y_{\mathrm{A}})^2 - d_{1\mathrm{A}}^2 = 0 \tag{iii}$$

$$\phi_2 \equiv (x_1 - x_2)^2 + (y_1 - y_2)^2 - d_{12}^2 = 0 \tag{iv}$$

$$\phi_3 \equiv (x_2 - x_{\mathrm{B}})^2 + (y_2 - y_{\mathrm{B}})^2 - d_{2\mathrm{B}}^2 = 0 \tag{v}$$

$$\phi_4 \equiv x_3 - x_1 + \frac{(x_2 - x_1)}{d_{12}}\,\overline{x}_3 - \frac{(y_2 - y_1)}{d_{12}}\,\overline{y}_3 = 0 \tag{vi}$$

$$\phi_5 \equiv y_3 - y_1 + \frac{(y_2 - y_1)}{d_{12}}\,\overline{x}_3 + \frac{(x_2 - x_1)}{d_{12}}\,\overline{y}_3 = 0 \tag{vii}$$

In addition to the geometric constraints, the designer also specifies the functional constraints. For the particular example being considered, we will impose the conditions of the trajectory of point 3 passing as close as possible to a finite set of design points (P_1, P_2, P_3, ..., P_N), as shown in Figure 10.20.

It is clear that each design point corresponds to a different value of the dependent coordinates vector $\mathbf{q}$. These values will be called ($\mathbf{q}^1$, $\mathbf{q}^2$, ..., $\mathbf{q}^N$). The functional constraints are now imposed for each design point. For a generic point i:

$$x_3^i - x_{P_i} = 0 \tag{viii}$$

$$y_3^i - y_{P_i} = 0 \tag{ix}$$

where $i = 1, 2, ..., N$.

In the general case, if $\mathbf{q}$ and $\mathbf{b}$ are the vectors of dependent coordinates and design variables, the geometric constraints equations can be expressed in vector form as

$$\mathbf{\Phi}(\mathbf{q}, \mathbf{b}) = 0 \tag{10.54}$$

Using natural coordinates, the constraints equations are very simple, and the design variables $\mathbf{b}$ appear explicitly in $\mathbf{\Phi}$. The constraint equations (10.54) differ from the ones considered in previous chapters because the parameters in $\mathbf{b}$ are not constant as before. They are true variables, because one is in the process of finding their optimum values.

The whole set of constraints for the design point i (geometric and functional) can be written as

$$\mathbf{\Phi}^i(\mathbf{q}^i, \mathbf{b}) = 0 \qquad i = 1, 2, ..., N \tag{10.55}$$

The *objective function* can now be introduced. Point 3 of the four-bar example should go exactly through the design points P_i. If it is not possible, a four-bar mechanism should be obtained whose dimensions guarantee that the error in getting these design points is minimum in some sense. Since exact solutions for the design problem may not exist, one must look for the optimal solution in the least square sense. One can define an objective function of the form:

$$\Psi(\mathbf{q}^1, \mathbf{q}^2, \ldots, \mathbf{q}^N, \mathbf{b}) = \frac{1}{2} \sum_{i=1}^{N} \mathbf{\Phi}^{iT}(\mathbf{q}^i, \mathbf{b})\ \mathbf{\Phi}^i(\mathbf{q}^i, \mathbf{b}) \tag{10.56}$$

or in a more compact form,

$$\Psi(\bar{\mathbf{q}}, \mathbf{b}) = \frac{1}{2}\ \bar{\mathbf{\Phi}}(\bar{\mathbf{q}}, \mathbf{b})^T\, \bar{\mathbf{\Phi}}(\bar{\mathbf{q}}, \mathbf{b}) \tag{10.57}$$

where $\bar{\mathbf{q}}$ is the vector $\bar{\mathbf{q}}^T = \{\mathbf{q}^{1T}, \mathbf{q}^{2T}, \ldots, \mathbf{q}^{NT}\}$ and $\bar{\mathbf{\Phi}}$ is a vector that contains all the geometry and functional constraints. The optimum design problem consists in minimizing the objective function Ψ with respect to vectors $\bar{\mathbf{q}}$ and $\mathbf{b}$, that is,

$$\min_{\bar{\mathbf{q}},\,\mathbf{b}} \Psi\,(\bar{\mathbf{q}},\mathbf{b}) = \frac{1}{2}\,\bar{\mathbf{\Phi}}(\bar{\mathbf{q}},\mathbf{b})^{\mathrm{T}}\,\bar{\mathbf{\Phi}}(\bar{\mathbf{q}},\mathbf{b}) \tag{10.58}$$

Differentiating with respect to $\bar{\mathbf{q}}$ and $\mathbf{b}$ and equating to zero, the following system of nonlinear equations is obtained:

$$\mathbf{J}(\bar{\mathbf{q}},\mathbf{b})\;\bar{\mathbf{\Phi}}(\bar{\mathbf{q}},\mathbf{b}) = 0 \tag{10.59}$$

where

$$\mathbf{J}(\bar{\mathbf{q}},\mathbf{b}) = \begin{bmatrix} \dfrac{\partial\bar{\mathbf{\Phi}}(\bar{\mathbf{q}},\mathbf{b})}{\partial\bar{\mathbf{q}}} \\ \dfrac{\partial\bar{\mathbf{\Phi}}(\bar{\mathbf{q}},\mathbf{b})}{\partial\mathbf{b}} \end{bmatrix} \tag{10.60}$$

The system of nonlinear equations (10.59) may now be solved by a quasi-Newton method. Expanding $\bar{\mathbf{\Phi}}(\bar{\mathbf{q}},\mathbf{b})$ in Taylor's series¿

$$\bar{\mathbf{\Phi}}(\bar{\mathbf{q}} + \Delta\bar{\mathbf{q}},\ \mathbf{b} + \Delta\mathbf{b}) = \bar{\mathbf{\Phi}}(\bar{\mathbf{q}},\ \mathbf{b}) + \mathbf{J}^{\mathrm{T}}\begin{Bmatrix}\Delta\bar{\mathbf{q}}\\ \Delta\mathbf{b}\end{Bmatrix} + \cdots \tag{10.61}$$

and substituting in equation (10.59), on can obtain

$$\mathbf{J}(\bar{\mathbf{q}},\mathbf{b})\,\bar{\mathbf{\Phi}}(\bar{\mathbf{q}},\mathbf{b}) + \mathbf{J}(\bar{\mathbf{q}},\mathbf{b})\,\mathbf{J}^{\mathrm{T}}(\bar{\mathbf{q}},\mathbf{b})\begin{Bmatrix}\Delta\bar{\mathbf{q}}\\ \Delta\mathbf{b}\end{Bmatrix} = 0 \tag{10.62}$$

from which the following iterative expression can be obtained:

$$\begin{Bmatrix}\bar{\mathbf{q}}\\ \mathbf{b}\end{Bmatrix}_{k+1} = \begin{Bmatrix}\bar{\mathbf{q}}\\ \mathbf{b}\end{Bmatrix}_{k} - \left[\mathbf{J}(\bar{\mathbf{q}},\mathbf{b})\,\mathbf{J}^{\mathrm{T}}(\bar{\mathbf{q}},\mathbf{b})\right]_{k}^{-1}\mathbf{J}(\bar{\mathbf{q}},\mathbf{b})_{k}\,\bar{\mathbf{\Phi}}(\bar{\mathbf{q}},\mathbf{b})_{k} \tag{10.63}$$

This method is sufficiently simple and general to be applied to nearly any system topology such as planar and three-dimensional, open- and closed-chains, with any number and kind of joints and bodies. This method can accommodate any kind of functional constraints, even a mixed set.

Example 10.4

The complete set of constraint equations will now be found for the four-bar mechanism of Example 10.1 considering five design points. Particularizing equations (iii)-(vii) and (viii)-(ix) for the generic design point P_i:

$$(x_1^{\mathrm{i}} - x_{\mathrm{A}})^2 + (y_1^{\mathrm{i}} - y_{\mathrm{A}})^2 - d_{1\mathrm{A}}^2 = 0 \tag{i}$$

$$(x_1^{\mathrm{i}} - x_2^{\mathrm{i}})^2 + (y_1^{\mathrm{i}} - y_2^{\mathrm{i}})^2 - d_{12}^2 = 0 \tag{ii}$$

$$(x_2^{\mathrm{i}} - x_{\mathrm{B}})^2 + (y_2^{\mathrm{i}} - y_{\mathrm{B}})^2 - d_{2\mathrm{B}}^2 = 0 \tag{iii}$$

$$-(1 + \bar{x}_3/d_{12})\,x_1^{\mathrm{i}} + (\bar{y}_3/d_{12})\,y_1^{\mathrm{i}} + (\bar{x}_3/d_{12})\,x_2^{\mathrm{i}} - (\bar{y}_3/d_{12})\,y_2^{\mathrm{i}} + x_3^{\mathrm{i}} = 0 \tag{iv}$$

$$-(\bar{y}_3/d_{12})\,x_1^{\mathrm{i}} - (1 + \bar{x}_3/d_{12})\,y_1^{\mathrm{i}} + (\bar{y}_3/d_{12})\,x_2^{\mathrm{i}} + (\bar{x}_3/d_{12})\,y_2^{\mathrm{i}} + y_3^{\mathrm{i}} = 0 \tag{v}$$

$$x_3^i - x_{P_i} = 0 \tag{vi}$$

$$y_3^i - y_{P_i} = 0 \tag{vii}$$

for *i = 1, 2, ..., 5*. There are *35* constraint equations. The number of unknowns is also *35*: five values of the six-element dependent coordinates vector $\mathbf{q}^i$ plus the five elements of the design variables vector **b**. With five design points, it is possible to get a mechanism that exactly satisfies the functional constraints. If there are more than five design points, only an optimal solution in the least square sense can be obtained.

10.5 Sensitivity Analysis and Optimization

The subject of the previous sections in this book has been the study of methods for analysis that constitute the basis simulation programs. These simulate the behavior of a multibody system once all of its geometric and dynamic characteristic have been defined. The analysis programs are certainly very useful. At the present time they are the only general purpose tools available for the largest number of applications. Currently, *design programs* are becoming more important. These programs will not only perform system analyses but also modify automatically its parameters so as to obtain an optimal behavior. An intermediate step between the analysis and optimal design programs are the *sensitivity analyses* which determine the variation of the response of the system in relation to each of the *design variables*.

The optimal design of a multibody system is started by defining an *objective function* which will optimize the system performance. The solution to the problem will be the configuration that minimizes the objective function in relation to the design variables. The problem may or may not have *design constraint equations*, that is, equalities or inequalities that should comply with certain specific functions of the design variables. The constraint equations mathematically introduce certain physical design limitations into the problem. For example, there cannot be any elements with negative mass or length, geometric limitations in the workspace, and so forth. The objective functions are defined depending on the application. Since the dynamics is a process that takes place over a period of time, the objective function is often defined as the integral of a specific function over a period of time or as a series of conditions that the multibody system must satisfy within certain intervals of time or at specific moments. The objective function depends on the design variables not only directly but also through the results of the dynamic analysis such as: positions, velocities, accelerations, stresses, and reactions.

Several optimization methods that minimize the objective function have been proposed (Gottfried and Weisman (1973), Haug and Arora (1979), Reklaitis et al. (1983)) . Almost all of the methods are based on the knowledge of the derivatives of the objective function with respect to the design variables. The determi-

nation of these derivatives is known as *sensitivity analysis* and is the first phase in the optimization process which may also be considered separately. Sensitivity analysis, which determines the tendencies of the objective function with respect to design variations, is also very useful in a non-automatic interactive design process. The derivatives of the objective function with respect to the design variables are calculated by means of the derivatives of the dynamic response with respect to positions, velocities, accelerations, stresses, and reactions.

The optimal design of multibody systems is undoubtedly an important problem, although it has not yet attained the level required for a general commercial implementation. Still, the calculation times are excessively high for even cases of average complexity, and there are important formulation and implementation problems that remain to be solved. For the time being, an interactive design based on analysis methods and sensitivity studies seems to be the most suitable alternative for general use. In this sensitivity analysis, the general ideas of Chang and Nikravesh (1985) will be followed.

First the sensitivities of the kinematic equations will be considered with respect to variations of the design variables $\delta\mathbf{b}$. As introduced in Chapter 2, the constraint equations are expressed as

$$\boldsymbol{\Phi} \equiv \boldsymbol{\Phi}(\mathbf{q}, t) = 0 \tag{10.64}$$

By simple differentiation, the velocity and acceleration constraint conditions can be found to be:

$$\dot{\boldsymbol{\Phi}} \equiv \boldsymbol{\Phi}_{\mathbf{q}}\, \dot{\mathbf{q}} + \boldsymbol{\Phi}_t = 0 \tag{10.65}$$

$$\ddot{\boldsymbol{\Phi}} \equiv \boldsymbol{\Phi}_{\mathbf{q}}\, \ddot{\mathbf{q}} - \boldsymbol{\gamma} = 0 \tag{10.66}$$

$$\boldsymbol{\gamma} = -(\boldsymbol{\Phi}_{\mathbf{q}}\dot{\mathbf{q}})_{\mathbf{q}} - 2\,\boldsymbol{\Phi}_{\mathbf{q}t}\,\dot{\mathbf{q}} - \boldsymbol{\Phi}_{tt} \tag{10.67}$$

The vector of dependent coordinates $\mathbf{q}$ will now be considered as a function of time t and also of the design variables $\mathbf{b}$. If a variation $\delta\mathbf{b}$ of the design variables is allowed, the following series expansion can be written:

$$\mathbf{q}(t, \mathbf{b} + \delta\mathbf{b}) = \mathbf{q}(t, \mathbf{b}) + \mathbf{q}_{\mathbf{b}}\,\delta\mathbf{b} + \ldots \tag{10.68}$$

and as a consequence the first variation of the positions, velocities, and accelerations become:

$$\delta\mathbf{q} = \mathbf{q}_{\mathbf{b}}\,\delta\mathbf{b} \tag{10.69}$$

$$\delta\dot{\mathbf{q}} = \dot{\mathbf{q}}_{\mathbf{b}}\,\delta\mathbf{b} \tag{10.70}$$

$$\delta\ddot{\mathbf{q}} = \ddot{\mathbf{q}}_{\mathbf{b}}\,\delta\mathbf{b} \tag{10.71}$$

Taking into account equation (10.69), the first variation of the constraint equations become

$$\mathbf{\Phi_q\, q_b}\ \delta\mathbf{b} + \mathbf{\Phi_b}\,\delta\mathbf{b} = (\mathbf{\Phi_q\, q_b} + \mathbf{\Phi_b})\,\delta\mathbf{b} = 0 \tag{10.72}$$

Since the variation $\delta\mathbf{b}$ is arbitrary, it can be concluded that

$$\mathbf{\Phi_q\, q_b} + \mathbf{\Phi_b} = 0 \tag{10.73}$$

Expression (10.73) is the equation that models the variation of the position vector $\mathbf{q}$ with respect to the design variables $\mathbf{b}$. The term $\mathbf{q_b}$ represents a matrix of partial derivatives. Similarly, the first variation of the velocity and acceleration constraint equations becomes:

$$\mathbf{\Phi_q}\,\dot{\mathbf{q}}_\mathbf{b} + \mathbf{\Phi_{qq}\, q_b}\,\dot{\mathbf{q}} + \mathbf{\Phi_{qb}}\,\dot{\mathbf{q}} + \mathbf{\Phi}_{t\mathbf{q}}\,\mathbf{q_b} + \mathbf{\Phi}_{t\mathbf{b}} = 0 \tag{10.74}$$

$$\begin{gathered}\mathbf{\Phi_q}\,\ddot{\mathbf{q}}_\mathbf{b} + \mathbf{\Phi_{qq}\, q_b}\,\ddot{\mathbf{q}} + \mathbf{\Phi_{qb}}\,\ddot{\mathbf{q}} + \dot{\mathbf{\Phi}}_\mathbf{qq}\,\mathbf{q_b}\,\dot{\mathbf{q}} + \\ + \dot{\mathbf{\Phi}}_\mathbf{qb}\,\dot{\mathbf{q}} + \dot{\mathbf{\Phi}}_\mathbf{q}\,\dot{\mathbf{q}}_\mathbf{b} + \dot{\mathbf{\Phi}}_{t\mathbf{q}}\,\mathbf{q_b} + \mathbf{\Phi}_{t\mathbf{b}} = 0\end{gathered} \tag{10.75}$$

Equations (10.73) to (10.75) allow one to compute the sensitivities of the kinematic constraint equations. Turn now to the variation of the equations of motion. To this end one can consider the Lagrange multiplier version of the equations of motion (equation (5.10)):

$$\mathbf{M}\,\ddot{\mathbf{q}} + \mathbf{\Phi}_\mathbf{q}^\mathrm{T}\,\boldsymbol{\lambda} = \mathbf{Q} \tag{10.76}$$

Taking into account that the first variation of the Lagrange multipliers is

$$\delta\boldsymbol{\lambda} = \boldsymbol{\lambda}_\mathbf{b}\,\delta\mathbf{b} \tag{10.77}$$

it becomes easy to see that the variation of (10.76) with respect to $\mathbf{b}$ is

$$\begin{gathered}\mathbf{M}\,\ddot{\mathbf{q}}_\mathbf{b} + \mathbf{\Phi}_\mathbf{q}^\mathrm{T}\,\boldsymbol{\lambda}_\mathbf{b} = \\ = \mathbf{Q_b} + \mathbf{Q_q\, q_b} + \mathbf{Q}_{\dot{\mathbf{q}}}\,\dot{\mathbf{q}}_\mathbf{b} - \mathbf{M_b}\,\ddot{\mathbf{q}} - \mathbf{\Phi}_\mathbf{qq}^\mathrm{T}\,\mathbf{q_b}\,\boldsymbol{\lambda} - \mathbf{\Phi}_\mathbf{qb}^\mathrm{T}\,\boldsymbol{\lambda}\end{gathered} \tag{10.78}$$

Equations (10.75) and (10.78) can be expressed jointly in the following form:

$$\begin{bmatrix} \mathbf{M} & \mathbf{\Phi}_\mathbf{q}^\mathrm{T} \\ \mathbf{\Phi_q} & \mathbf{0} \end{bmatrix} \begin{Bmatrix} \ddot{\mathbf{q}}_\mathbf{b} \\ \boldsymbol{\lambda}_\mathbf{b} \end{Bmatrix} = \begin{Bmatrix} \overline{\mathbf{Q}}_\mathbf{b} \\ \overline{\mathbf{c}}_\mathbf{b} \end{Bmatrix} \tag{10.79}$$

where

$$\overline{\mathbf{Q}}_\mathbf{b} = \mathbf{Q_b} + \mathbf{Q_q\, q_b} + \mathbf{Q}_{\dot{\mathbf{q}}}\,\dot{\mathbf{q}}_\mathbf{b} - \mathbf{M_b}\,\ddot{\mathbf{q}} - \mathbf{\Phi}_\mathbf{qq}^\mathrm{T}\,\mathbf{q_b}\,\boldsymbol{\lambda} - \mathbf{\Phi}_\mathbf{qb}^\mathrm{T}\,\boldsymbol{\lambda} \tag{10.80}$$

$$\begin{gathered}\overline{\mathbf{c}}_\mathbf{b} = -\,\mathbf{\Phi_{qq}\, q_b}\,\ddot{\mathbf{q}} - \mathbf{\Phi_{qb}}\,\ddot{\mathbf{q}} - \dot{\mathbf{\Phi}}_\mathbf{qq}\,\mathbf{q_b}\,\dot{\mathbf{q}} - \\ - \dot{\mathbf{\Phi}}_\mathbf{qb}\,\dot{\mathbf{q}} - \dot{\mathbf{\Phi}}_\mathbf{q}\,\dot{\mathbf{q}}_\mathbf{b} - \dot{\mathbf{\Phi}}_{t\mathbf{q}}\,\mathbf{q_b} - \mathbf{\Phi}_{t\mathbf{b}}\end{gathered} \tag{10.81}$$

Equation (10.79) closely resembles the general form of the equations of motion (5.10):

$$\begin{bmatrix} \mathbf{M} & \boldsymbol{\Phi}_{\mathbf{q}}^{\mathrm{T}} \\ \boldsymbol{\Phi}_{\mathbf{q}} & \mathbf{0} \end{bmatrix} \begin{Bmatrix} \ddot{\mathbf{q}} \\ \boldsymbol{\lambda} \end{Bmatrix} = \begin{Bmatrix} \mathbf{Q} \\ -\dot{\boldsymbol{\Phi}}_{\mathrm{t}} - \dot{\boldsymbol{\Phi}}_{\mathbf{q}}\, \dot{\mathbf{q}} \end{Bmatrix} \tag{10.82}$$

The set of linear equations (10.79) and (10.82) have a common matrix of coefficients, and therefore only one Gauss decomposition is necessary. Equation (10.82) must be solved first to obtain $\mathbf{q}$ and $\boldsymbol{\lambda}$ that appear in the RHS of (10.79). This last equation has as many unknowns as design variables. The position and velocity sensitivities may be obtained from those of the accelerations through numerical integration. The possible instabilities arising from the integration process may be eliminated by solving the system of mixed differential and algebraic equations (See Chapter 7) or by using the Baumgarte stabilization (See Chapter 5).

A third way to avoid the instabilities is through the use of independent variables, as explained in Section 5.2. It is possible to define a matrix of independent sensitivities that according to equations (5.64) and (5.61) must satisfy the following relation:

$$\dot{\mathbf{z}}_{\mathbf{b}} = \mathbf{B}\, \dot{\mathbf{q}}_{\mathbf{b}} \tag{10.83}$$

where

$$\dot{\mathbf{q}}_{\mathbf{b}} = \begin{bmatrix} \boldsymbol{\Phi}_{\mathbf{q}} \\ \mathbf{B} \end{bmatrix}^{-1} \begin{Bmatrix} \boldsymbol{\gamma}_{\mathbf{b}} \\ \dot{\mathbf{z}}_{\mathbf{b}} \end{Bmatrix} \equiv \begin{bmatrix} \mathbf{S} & \mathbf{R} \end{bmatrix} \begin{Bmatrix} \boldsymbol{\gamma}_{\mathbf{b}} \\ \dot{\mathbf{z}}_{\mathbf{b}} \end{Bmatrix} = \mathbf{S}\, \boldsymbol{\gamma}_{\mathbf{b}} + \mathbf{R}\, \dot{\mathbf{z}}_{\mathbf{b}} \tag{10.84}$$

$$\boldsymbol{\gamma}_{\mathbf{b}} = -\boldsymbol{\Phi}_{\mathbf{q}\mathbf{q}}\, \mathbf{q}_{\mathbf{b}}\, \dot{\mathbf{q}} - \boldsymbol{\Phi}_{\mathbf{q}\mathbf{b}}\, \dot{\mathbf{q}} - \boldsymbol{\Phi}_{t\mathbf{q}}\, \mathbf{q}_{\mathbf{b}} - \boldsymbol{\Phi}_{t\mathbf{b}} \tag{10.85}$$

Taking into account equation (10.81), the sensitivities for accelerations become:

$$\ddot{\mathbf{z}}_{\mathbf{b}} = \mathbf{B}\, \ddot{\mathbf{q}}_{\mathbf{b}} \tag{10.86}$$

$$\ddot{\mathbf{q}}_{\mathbf{b}} = \begin{bmatrix} \boldsymbol{\Phi}_{\mathbf{q}} \\ \mathbf{B} \end{bmatrix}^{-1} \begin{Bmatrix} \bar{\mathbf{c}}_{\mathbf{b}} \\ \ddot{\mathbf{z}}_{\mathbf{b}} \end{Bmatrix} \equiv \begin{bmatrix} \mathbf{S} & \mathbf{R} \end{bmatrix} \begin{Bmatrix} \bar{\mathbf{c}}_{\mathbf{b}} \\ \ddot{\mathbf{z}}_{\mathbf{b}} \end{Bmatrix} = \mathbf{S}\, \bar{\mathbf{c}}_{\mathbf{b}} + \mathbf{R}\, \ddot{\mathbf{z}}_{\mathbf{b}} \tag{10.87}$$

Introducing (10.87) into (10.79), pre-multiplying the result by $\mathbf{R}^{\mathrm{T}}$, and taking into account that the columns of $\mathbf{R}$ are orthogonal to the rows of $\boldsymbol{\Phi}_{\mathbf{q}}$, one can get

$$\mathbf{R}^{\mathrm{T}}\, \mathbf{M}\, \mathbf{R}\, \ddot{\mathbf{z}}_{\mathbf{b}} = \mathbf{R}^{\mathrm{T}} (\overline{\mathbf{Q}}_{\mathbf{b}} - \mathbf{M}\, \mathbf{S}\, \bar{\mathbf{c}}_{\mathbf{b}}) \tag{10.88}$$

All the improved dynamic techniques described in Chapter 8 can be applied to the sensitivity equations (10.79) and (10.88). The most efficient formulations for the dynamic analysis may also be the basis of a very efficient computation of the sensitivities of the position, velocity, and acceleration vectors.

10.6 Singular Positions

The methods and results presented in this section are contributions from Bayo and Avello (1993).

A *singular position* is encountered when the multibody reaches a kinematic configuration in which there is a sudden change in the number of degrees of freedom. For instance, a slider-crank mechanism, as the one shown in Figure 10.21, reaches a singular position when the two links are in vertical position. In that configuration, both links are coincident, and the mechanism has not one but two degrees of freedom. These two degrees of freedom correspond to the two possible motions (bifurcations) that the mechanism can undergo (illustrated in Figure 10.22). Figure 10.22a shows the first possible motion that corresponds to a slider-crank mechanism. Figure 10.22b shows the second motion corresponding to a rotating bar (in fact two coincident rotating bars). Here, a singular position implies a *bifurcation* point, in which the mechanism can theoretically undergo different paths.

The existence of a singular position with both the classical Lagrange multipliers approach and the use of independent coordinates is invariably detected when the Jacobian matrix of the constraints becomes rank-deficient. These formulations are based on the decomposition of the Jacobian matrix. Since its rank suddenly falls at a singular position, the decomposition fails and therefore no solution can be found. The simulation then may crash not because of the physics of the problem but because of the inability of the dynamic formulation to overcome the sudden change in the rank of the Jacobian matrix.

Equation (5.10) is the key equation for the solution of the dynamics using the Lagrange multipliers method. This equation is again written as

$$\begin{bmatrix} \mathbf{M} & \mathbf{\Phi}_{\mathbf{q}}^{\mathrm{T}} \\ \mathbf{\Phi}_{\mathbf{q}} & \mathbf{0} \end{bmatrix} \begin{Bmatrix} \ddot{\mathbf{q}} \\ \boldsymbol{\lambda} \end{Bmatrix} = \begin{Bmatrix} \mathbf{Q} \\ \mathbf{c} \end{Bmatrix} \tag{10.89}$$

Assuming that all the constraints are independent, that is if (m=n–f), the rank of the leading matrix in this equations is (n+m). Since the Jacobian matrix becomes rank-deficient in singular positions, this matrix becomes singular. The accelerations cannot be computed, and the dynamic simulation may either crash or introduce large errors at this point. Equation (5.67) is the alternate key equation for the independent coordinate method, which can be rewritten again as

$$\mathbf{R}^{\mathrm{T}}\,\mathbf{M}\,\mathbf{R}\,\ddot{\mathbf{z}} = \mathbf{R}^{\mathrm{T}}\,\mathbf{Q} - \mathbf{R}^{\mathrm{T}}\,\mathbf{M}\,\mathbf{S}\,\mathbf{c} \tag{10.90}$$

When a singular position is reached, the computation of the matrix $\mathbf{R}$ fails, because the Jacobian matrix becomes rank-deficient. Thus, it's decomposition can no longer be carried out.

If a singular position is not exactly reached, the leading matrix of both methods will not be strictly singular but quasi-singular with a very high condition number. If this situation is not correctly tracked, the integration and round-off errors will be amplified, and the resulting solutions may be totally erroneous. A

partial solution to the problem of singular positions was provided by Park and Haug (1988) with a method that detects the ill-conditioning of the Jacobian matrix so that the integrator can step over it. Ider and Amirouche (1989) and Amirouche and Chin-Wei (1990) proposed a *regularization method* to cope with singularities. Roughly, the idea consists in substituting the linearly dependent rows of the Jacobian matrix by their derivatives, which turns the Jacobian matrix non-singular.

The penalty-augmented Lagrangian formulation provides a nice solution to this problem. A more detailed exposition of the following analysis is presented by Bayo and Avello (1993). The key equation for the augmented Lagrangian formulation (5.48) can be expressed as

$$\begin{aligned}(\mathbf{M} + \boldsymbol{\Phi}_{\mathbf{q}}^{\mathrm{T}}\, \boldsymbol{\alpha}\, \boldsymbol{\Phi}_{\mathbf{q}})\, \ddot{\mathbf{q}} = \\ = \mathbf{Q} - \boldsymbol{\Phi}_{\mathbf{q}}^{\mathrm{T}}\, \boldsymbol{\alpha}\, (\dot{\boldsymbol{\Phi}}_{\mathbf{q}}\, \dot{\mathbf{q}} + \dot{\boldsymbol{\Phi}}_{t} + 2\, \boldsymbol{\Omega}\, \boldsymbol{\mu}\, \dot{\boldsymbol{\Phi}} + \boldsymbol{\Omega}^{2}\, \boldsymbol{\Phi}) - \boldsymbol{\Phi}_{\mathbf{q}}^{\mathrm{T}}\, \boldsymbol{\lambda}^{*}\end{aligned} \tag{10.91}$$

It is important to note that there is a very important difference between equation (10.91) and those corresponding to the Lagrange multiplier and independent coordinates (10.89) and (10.90), respectively. The leading matrices of equations (10.89) and (10.90) become singular in singular positions. Although the mass matrix $\mathbf{M}$ is generally positive semi-definite, it is always strictly positive definite in the nullspace of the Jacobian matrix. A look at equation (10.91) reveals that its leading matrix $(\mathbf{M} + \boldsymbol{\Phi}_{\mathbf{q}}^{\mathrm{T}}\, \boldsymbol{\alpha}\, \boldsymbol{\Phi}_{\mathbf{q}})$ is always positive definite. It can always be factored, even in singular positions.

Remark. It is important at this stage to emphasize the difference between a singular Jacobian matrix and a singular position. While a singular position always implies a singular Jacobian matrix, the converse is not always true. A Jacobian matrix can become singular when redundant constraints are present, a dead-lock position is reached, or when the coordinate partitioning between dependent and independent coordinates is not made properly or has not been updated for a while. Contrary to the case of a singular position, these singularities can be avoided and the simulation may proceed smoothly. The difference between avoidable and unavoidable singular Jacobian matrices can be better understood by partitioning the columns of the Jacobian matrix $\boldsymbol{\Phi}_{\mathbf{q}}$ into two submatrices $\boldsymbol{\Phi}_{\mathbf{q}}^{\mathrm{d}}$ and $\boldsymbol{\Phi}_{\mathbf{q}}^{\mathrm{i}}$, corresponding to the dependent and independent coordinates, respectively. This partition is made so that $\boldsymbol{\Phi}_{\mathbf{q}}^{\mathrm{d}}$ has full row rank. When $\boldsymbol{\Phi}_{\mathbf{q}}^{\mathrm{d}}$ is rank-deficient but $\boldsymbol{\Phi}_{\mathbf{q}}$ has full row rank, the singularity is avoidable, since the full rank of $\boldsymbol{\Phi}_{\mathbf{q}}^{\mathrm{d}}$ can be recovered by a new suitable choice of independent coordinates. However, when $\boldsymbol{\Phi}_{\mathbf{q}}$ loses rank, the singularity is unavoidable. It is a physical singularity, and the rank of $\boldsymbol{\Phi}_{\mathbf{q}}^{\mathrm{d}}$ cannot be modified by any choice of the independent coordinates.

Example 10.5

To better understand the application of the augmented Lagrangian formulation in singular and non-singular positions, consider the slider-crank mechanism shown

Table 10.1. Convergence rate with $\alpha=10^4$.

Iteration #	Error
1	$6.5792\ 10^{-4}$
2	$4.3705\ 10^{-8}$
3	$2.9206\ 10^{-12}$
4	$1.6107\ 10^{-14}$

in Figure 10.21. Both links are of length $l=1$ m with a uniformly distributed mass of $m=1$ Kg. Take as position coordinates $\mathbf{q}$, the x and y coordinates of the crank end, and the x coordinate of the slider. Thus $\mathbf{q}^T=\{x_1, y_1, x_2\}$. One can consider the gravity force with a value $g=-9.81$ m/s^2 acting in the Y direction. The (3×3) mass matrix corresponding to these variables is

$$\mathbf{M} = \frac{1}{6}\begin{bmatrix} 4 & 0 & 1 \\ 0 & 4 & 0 \\ 1 & 0 & 2 \end{bmatrix}$$

This mechanism has one degree of freedom only. Therefore there are two geometrical constraints that correspond to the constant distance conditions:

$$\mathbf{\Phi} = \begin{Bmatrix} \frac{1}{2}\left(x_1^2 + y_1^2 - 1\right) & \frac{1}{2}\left[\left(x_2 - x_1\right)^2 + y_1^2 - 1\right] \end{Bmatrix}$$

When the crank forms an angle of $\pi/2$ radians with the horizontal, the coupler is coincident with the crank. The crank axis is also coincident with the slider. In this position the mechanism has two instantaneous degrees of freedom, since it can undergo either the motion of a slider-crank or the motion of two superimposed rotating bars. The augmented Lagrangian formulation (Algorithm 5-3) can now be applied for the instantaneous solution of the accelerations for both a nonsingular position and a singular position.

Nonsingular Position. Consider the mechanism in an initial position in which the crank forms an angle of $\pi/4$ with the horizontal and in which the slider has a velocity $\dot{x}_2 = -2$ m/s. The exact acceleration has been computed first with the classical Lagrange multiplier method of equation (10.89). The accelerations have been calculated with the Algorithm 5-3, using equation (10.91) iteratively with a value $\alpha=10^4$. Table 10.1 shows the norm of the difference between the exact acceleration and the one obtained with augmented Lagrangian formulation.

Table 10.1 also shows that the convergence rate of the iterative algorithm is considerably fast. A higher penalty value gives a faster convergence rate but a lower precision. For instance, a penalty value of $\alpha=10^7$ yields an error on the order of 10^{-12} in one iteration. Further iterations are unable to improve the solution, since some precision is lost in floating-point arithmetic operations between numbers with exponents of significantly different values.

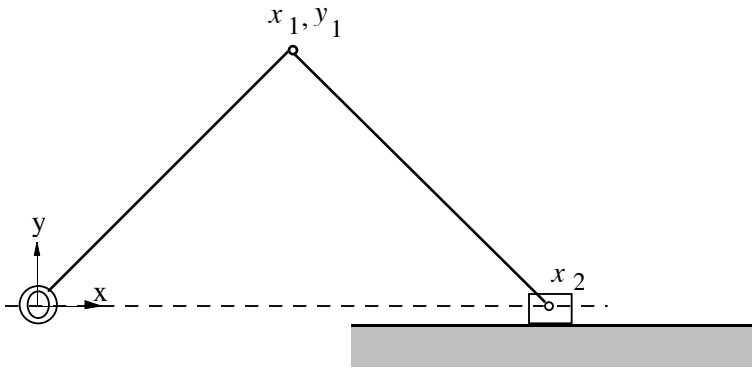

Figure 10.21. Slider-crank mechanism

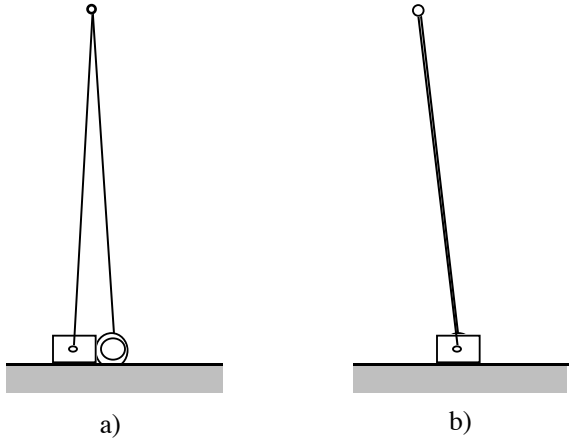

Figure 10.22. Possible bifurcations: (a) slider-crank mechanism motion, (b) rotating bar motion

Singular Position. Consider the crank in a vertical position, forming an angle of $\pi/2$ radians with the horizontal. As was done in the nonsingular case, the slider velocity takes the value $\dot{x}_2 = -2$ m/s. Since the mechanism is in a singular position with two instantaneous degrees of freedom, the horizontal velocity of the crank end also has to be specified. It can be easily shown that, theoretically, the crank end can have any velocity value $\dot{x}_1 = v$. However, the slider-crank motion must satisfy the condition $x_1 = x_2/2$ over all its motion. Therefore the velocity $\dot{x}_1 = -1$ seems the obvious choice. In this example, the choice for the crank-end velocity is being made explicitly, but during a dynamic simulation, the numerical integrator will provide this value. Since the integrator assumes a continuous variation of the variables, this condition will be automatically guaranteed.

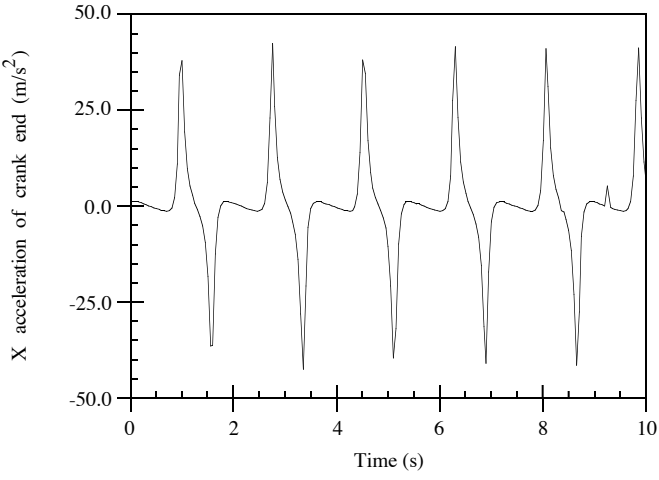

(a)

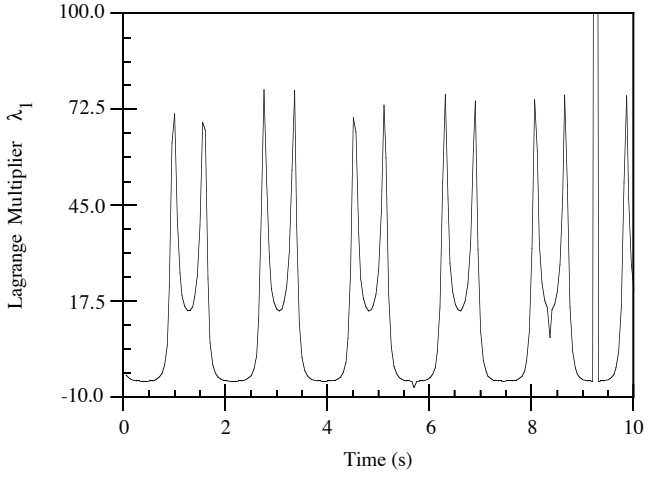

(b)

Figure 10.23. Acceleration-based augmented Lagrangian formulation: (a) acceleration of the crank-end; (b) Lagrange multiplier.

In this case, the exact acceleration value cannot be computed with equation (10.89), because the leading matrix is singular. However, the application of equation (10.91) with a value of α=10^4 leads to

$$\begin{bmatrix} \frac{2}{3} & 0 & \frac{1}{6} \\ 0 & 2\left(10^4+\frac{1}{3}\right) & 0 \\ \frac{1}{6} & 0 & \frac{1}{3} \end{bmatrix} \begin{Bmatrix} \ddot{x}_1 \\ \ddot{y}_1 \\ \ddot{x}_2 \end{Bmatrix} = \begin{Bmatrix} 0 \\ -(2\cdot 10^4+9.81) \\ 0 \end{Bmatrix}$$

which can be inverted and leads to the solution (0, –1.00047382543624272, 0). After three iterations, the result is (0,–1,0) which is accurate to 14 digits.

This example clearly and simply illustrates that the augmented Lagrangian formulation works in singular positions; whereas the classical formulations such as the Lagrange multipliers method or the reduction to independent coordinates fail.

An interesting finding is the augmented Lagrangian formulation in its canonical form defined by equation (5.119):

$$\begin{aligned} &\left(\mathbf{M} + \boldsymbol{\Phi}_{\mathbf{q}}^{\mathrm{T}}\,\boldsymbol{\alpha}\,\boldsymbol{\Phi}_{\mathbf{q}}\right)\dot{\mathbf{q}} = \\ &= \mathbf{p} - \boldsymbol{\Phi}_{\mathbf{q}}^{\mathrm{T}}\,\boldsymbol{\alpha}\left(\boldsymbol{\Phi}_t + 2\boldsymbol{\mu}\,\boldsymbol{\Omega}\,\boldsymbol{\Phi} + \boldsymbol{\Omega}^2\int_{t_o}^{t}\boldsymbol{\Phi}\,d\tau\right) - \boldsymbol{\Phi}_{\mathbf{q}}^{\mathrm{T}}\,\boldsymbol{\sigma}^{*} \end{aligned} \tag{10.92}$$

This formulation is more effective and reliable than its acceleration-based counterpart (equation 10.91) under singular positions. In fact, while both formulations require the triangularization of the same leading matrix for each function evaluation, there are advantages in the use of the canonical as compared to the acceleration. The kinematic constraint conditions are differentiated only once with the canonical procedure but twice in the acceleration-based formulation. This will lead to lesser violations of the constraints. The next example illustrates how this factor may become detrimental for the acceleration-based formulation under repetitive singular positions; whereas the canonical approach leads to a much better performance.

Example 10.6

Dynamic simulation of the slider-crank mechanism. Consider again the same slider-crank mechanism in an initial position so that the crank forms an angle of $\pi/4$ radians with the X axis and that the slider's velocity is $\dot{x}_2 = -4$ m/s. By integrating the equations of motion for a total of 10 seconds, a dynamic simulation is performed using a conditionally stable variable step and order integrator based on predictor-corrector multistep formulae (Shampine and Gordon (1975)). The error tolerance is set to 10^{-5} and penalty parameters $\alpha = 10^7$, $\Omega = 10$, and $\mu = 1$ are chosen. During the simulation, the mechanism goes through the singular position eleven times following a periodical response.

First, the simulation was carried out with the acceleration-based Algorithm 5-3 (equation (10.91)). Figure 10.24a shows the X acceleration of the crank-end over the time period of 10 seconds. Figure 10.24b shows the value of the Lagrange multiplier λ_1 corresponding to the constant distance constraint condition between the crank axis and the crank end. A very interesting point can be brought up from

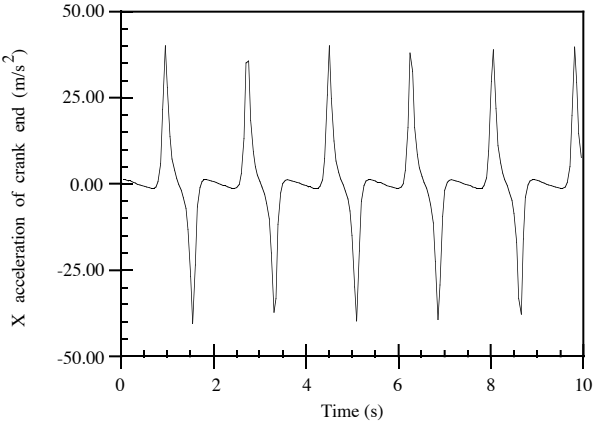

(a)

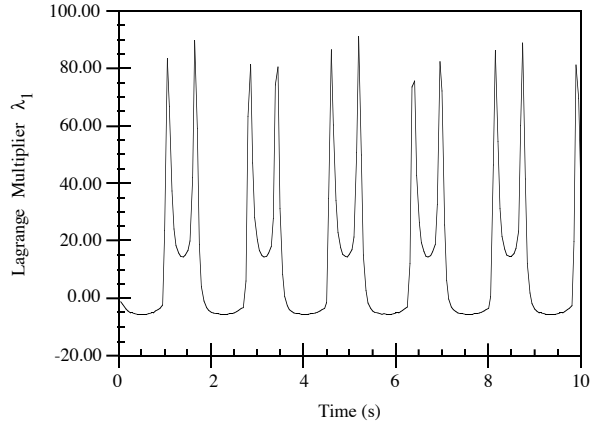

(b)

Figure 10.24. Canonical-based augmented Lagrangian formulation: (a) acceleration of the crank-end; (b) Lagrange multiplier.

these figures. The value of the acceleration of the crank-end and λ_1 presents spikes around t=9.25s. The cause of this phenomenon is the violation of the constraints around the singular position, due to the combination of the errors produced by the numerical integration routine and by the round-off errors produced by augmented Lagrangian procedure. These errors are more critical in the acceleration-based algorithm because the constraint equations are differentiated twice.

The simulation is repeated, using the Algorithm 5-8 (canonical formulation) with the same error tolerance and values for the penalty parameters. This time, the

values of λ_1 and the crank-end acceleration, illustrated in Figures 24a and 24b, no longer show the spikes shown in Figure 10.23. The accumulation of small constraint violations in the neighborhood of the singular position is the cause for the sudden peaks and jumps in the constraint forces and accelerations produced in Figure 10.23. The better results obtained with the canonical formulation are due to its better constraint stabilization properties that make this algorithm better suited for problems in which the constraint violation must be effectively stabilized, as is the case of the analysis of singular positions.

The way the acceleration-based augmented Lagrangian formulation may be improved, if it is to be used in repetitive singular positions, is by setting tighter error tolerances and raising the value of the parameter Ω. However, this will introduce numerical stiffness in the problem and will increase the computational effort. In this example, the value of ω =20 solves the problem satisfactorily at the cost of a lengthier and more costly integration.

References

Alvarez, G. and Jiménez, J.M., "A Simple and General Method for Kinematic Synthesis of Spatial Mechanisms", to be published, (1993)

Amirouche, F.M.L. and Chin-Wei, T., "Regularization and Stability of the Constraints in the Dynamics of Multibody Systems", *Nonlinear Dynamics*, Vol. 1, pp. 459-475, (1990).

Angeles, J., *Spatial Kinematic Chains*, Springer-Verlag, (1982).

Avilés, R., Ajuria, M.B. and García de Jalón, J., "A Fairly General Method for Optimum Synthesis of Planar Mechanisms", *Mechanism and Machine Theory*, Vol. 20, pp. 321-328, (1985).

Bagci, C., "Dynamic Motion Analysis of Plane Mechanisms with Coulomb and Viscous Damping Via the Joint Force Analysis", *ASME Journal of Engineering for Industry*, pp. 551-559, (1975).

Bayo, E. and Avello, A., "Singularity Free Augmented Lagrangian Algorithms for Constraint Multibody Dynamics", to appear in the *Journal of Nonlinear Dynamics*, (1993).

Chang, C.O. and Nikravesh, P.E., "Optimal Design of Mechanical Systems with Constraint Violation Stabilization Method", *ASME Journal of Mechanisms, Transmissions, and Automation in Design*, Vol. 107, pp. 493-498, (1985).

Dubowsky, S., Deck, J.F., and Costello, H., "The Dynamic Modeling of Flexible Spatial Machine Systems with Clearance Connections", *ASME Journal of Mechanisms, Transmissions, and Automation in Design*, Vol. 109, pp. 87-94, (1987).

Erdman, A.G. and Sandor, G.N., *Mechanism Design: Analysis and Synthesis*, Volumes 1 and 2, Prentice-Hall, (1984).

Gottfried, B.S. and Weisman, J., *Introduction to Optimization Theory*, Prentice-Hall, (1973).

Haug, E.J. and Arora, J.S., *Applied Optimal Design. Mechanical and Structural Systems*, Wiley, (1979).

Haug, E.J., Wu, S.C., and Yang, S.M., "Dynamics of Mechanical Systems with Coulomb Friction, Stiction, Impact, and Constraint Addition-Deletion. I-Theory, II-Planar Systems, and III-Spatial Systems", *Mechanism and Machine Theory*, Vol. 21, pp. 401-425, (1986).

Ider, S.K. and Amirouche, F.M.L., "Numerical Stability of the Constraints Near Singular Positions in the Dynamics of Multibody Systems", *Computers and Structures*, Vol. 33, pp. 129-137, (1989).

Park, T. and Haug, E.J., "Ill-Conditioned Equations in Kinematics and Dynamics of Machines", *Int. Journal for Numerical Methods in Engineering*, Vol. 26, pp. 217-230, (1988).

Reklaitis, G.V., Ravindran, A., and Ragsdell, K.M., *Engineering Optimization. Methods and Applications*, Wiley, (1983).

Rooney, G.T. and Deravi, P., "Coulomb Friction in Mechanism Sliding Joints", *Mechanism and Machine Theory*, Vol. 17, pp. 207-211, (1982).

Shampine, L.F. and Gordon, M., *Computer Solution of Ordinary Differential Equations: the Initial Value Problem*, W.J. Freeman, San Francisco, (1975).

Suh, C.H. and Radcliffe, C.W., *Kinematics and Mechanism Design*, Wiley, (1978).

Threlfall, D.C., "The Inclusion of Coulomb Friction in Mechanisms Programs with Particular Reference to DRAM", *Mechanism and Machine Theory*, Vol. 13, pp. 475-483, (1978).